

# Constraining the Galaxy-Halo Connection Over The Last 13.3 Gyrs: Star Formation Histories, Galaxy Mergers and Structural Properties

Aldo Rodríguez-Puebla<sup>1,2\*</sup>, Joel R. Primack<sup>3</sup>, Vladimir Avila-Reese<sup>2</sup>,  
and S. M. Faber<sup>4</sup>

<sup>1</sup> *Department of Astronomy & Astrophysics, University of California at Santa Cruz, Santa Cruz, CA 95064, USA*

<sup>2</sup> *Instituto de Astronomía, Universidad Nacional Autónoma de México, A. P. 70-264, 04510, México, D.F., México*

<sup>3</sup> *Physics Department, University of California, Santa Cruz, CA 95064, USA*

<sup>4</sup> *UCO/Lick Observatory, Department of Astronomy and Astrophysics, University of California, Santa Cruz, CA 95064, USA*

## ABSTRACT

We present new determinations of the stellar-to-halo mass relation (SHMR) at  $z = 0 - 10$  that match the evolution of the galaxy stellar mass function, the SFR –  $M_*$  relation, and the cosmic star formation rate. We utilize a compilation of 40 observational studies from the literature and correct them for potential biases. Using our robust determinations of halo mass assembly and the SHMR, we infer star formation histories, merger rates, and structural properties for average galaxies, combining star-forming and quenched galaxies. Our main findings: (1) The halo mass  $M_{50}$  above which 50% of galaxies are quenched coincides with  $\text{sSFR}/\text{sMAR} \sim 1$ , where sMAR is the specific halo mass accretion rate. (2)  $M_{50}$  increases with redshift, presumably due to cold streams being more efficient at high redshift while virial shocks and AGN feedback become more relevant at lower redshifts. (3) The ratio  $\text{sSFR}/\text{sMAR}$  has a peak value, which occurs around  $M_{\text{vir}} \sim 2 \times 10^{11} M_{\odot}$ . (4) The stellar mass density within 1 kpc,  $\Sigma_1$ , is a good indicator of the galactic global sSFR. (5) Galaxies are statistically quenched after they reach a maximum in  $\Sigma_1$ , consistent with theoretical expectations of the gas compaction model; this maximum depends on redshift. (6) In-situ star formation is responsible for most galactic stellar mass growth, especially for lower-mass galaxies. (7) Galaxies grow inside out. The marked change in the slope of the size–mass relation when galaxies became quenched, from  $d \log R_{\text{eff}}/d \log M_* \sim 0.35$  to  $\sim 2.5$ , could be the result of dry minor mergers.

# Constraining the Galaxy Halo Connection: Star Formation

## Histories, Galaxy Mergers, and Structural Properties, by Aldo

Rodríguez-Puebla, Joel Primack, Vladimir Avila-Reese, and Sandra Faber

We use results from the Bolshoi-Planck simulation (Aldo Rodríguez-Puebla, Peter Behroozi, Joel Primack, Anatoly Klypin, Christoph Lee, Doug Hellinger, MNRAS 462, 893 (2016), including halo and subhalo abundance as a function of redshift (Fig B1 at right), median halo mass growth for halos of given  $M_{\text{vir}}$  at  $z = 0$  (Fig B2). Our semi-empirical approach uses SubHalo Abundance Matching (SHAM), which matches the cumulative galaxy stellar mass function (GSMF) to the cumulative stellar mass function to correlate galaxy stellar mass with (sub)halo mass.

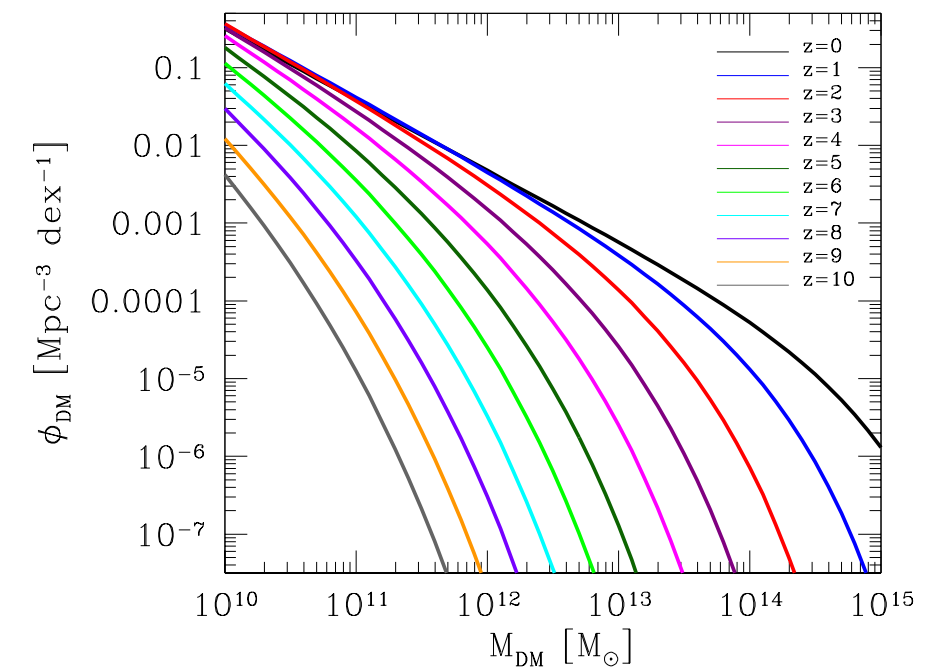
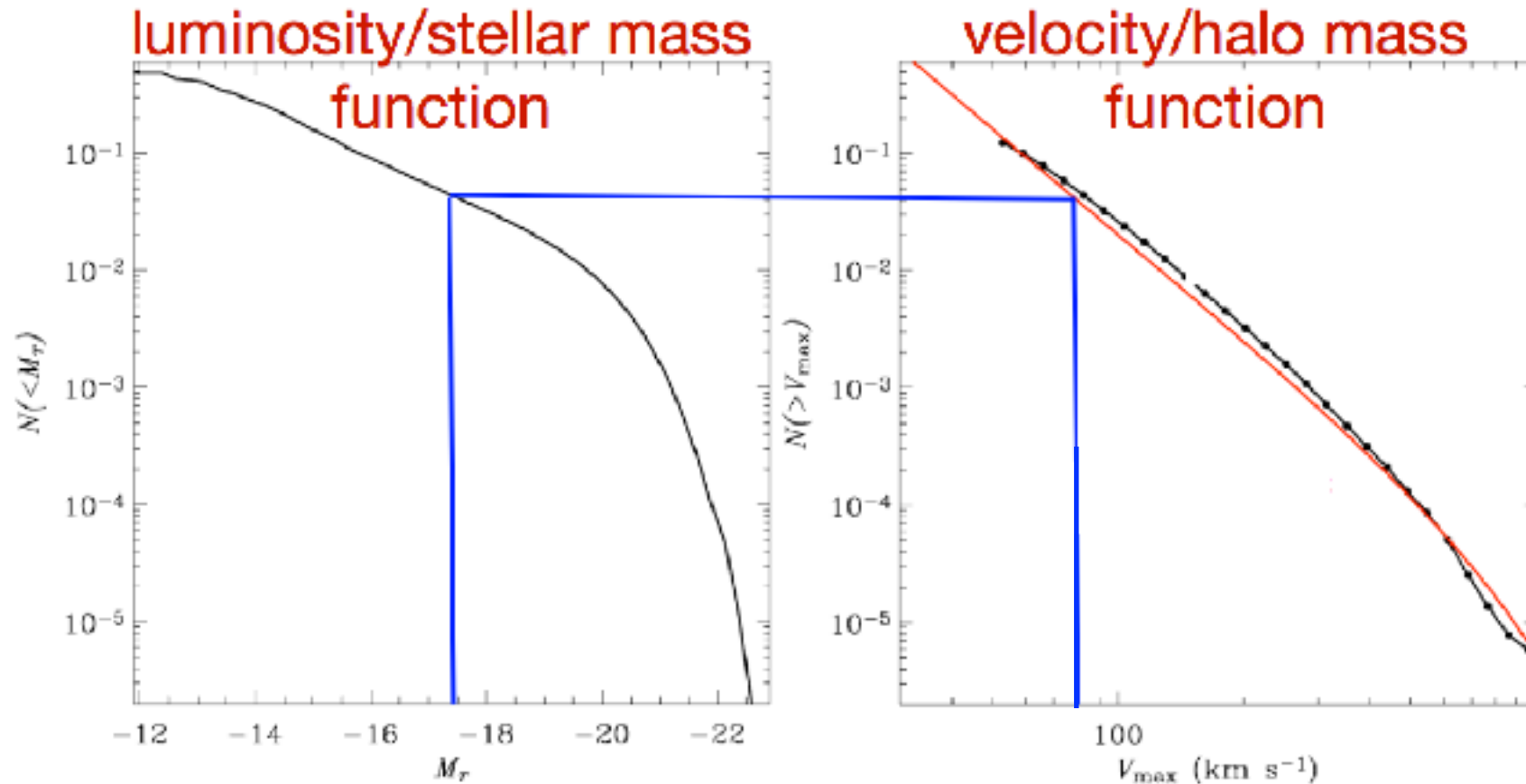


**Figure B1.** Total number density of halos and subhalos,  $\phi_{\text{halo}}(M_{\text{halo}})dM_{\text{halo}}$ , from  $z = 0$  to  $z = 10$ .  $M_{\text{halo}}$  should be interpreted as the virial mass,  $M_{\text{vir}}$ , for distinct halos and  $M_{\text{peak}}$  for subhalos. For central halos we are using the Tinker et al. (2008) model with the parameters updated in Rodríguez-Puebla et al. (2016a) based on large Bolshoi-Planck and MultiDark-Planck cosmological simulations using the cosmological parameters from the Planck mission. For subhalos we use the maximum mass reached along the main progenitor assembly, denoted as  $M_{\text{peak}}$ .



**Assumptions:** every halo hosts a galaxy, mass growth of galaxies is associated with that of halos, blue star-forming galaxies are Sersic  $n = 1$  (i.e., exponential) and red quenched galaxies are  $n = 4$  (de Vaucouleurs).

Unlike the halo occupation distribution (HOD) or conditional stellar mass function approaches, we do not attempt to match the galaxy two-point correlation function or galaxy group catalogs.

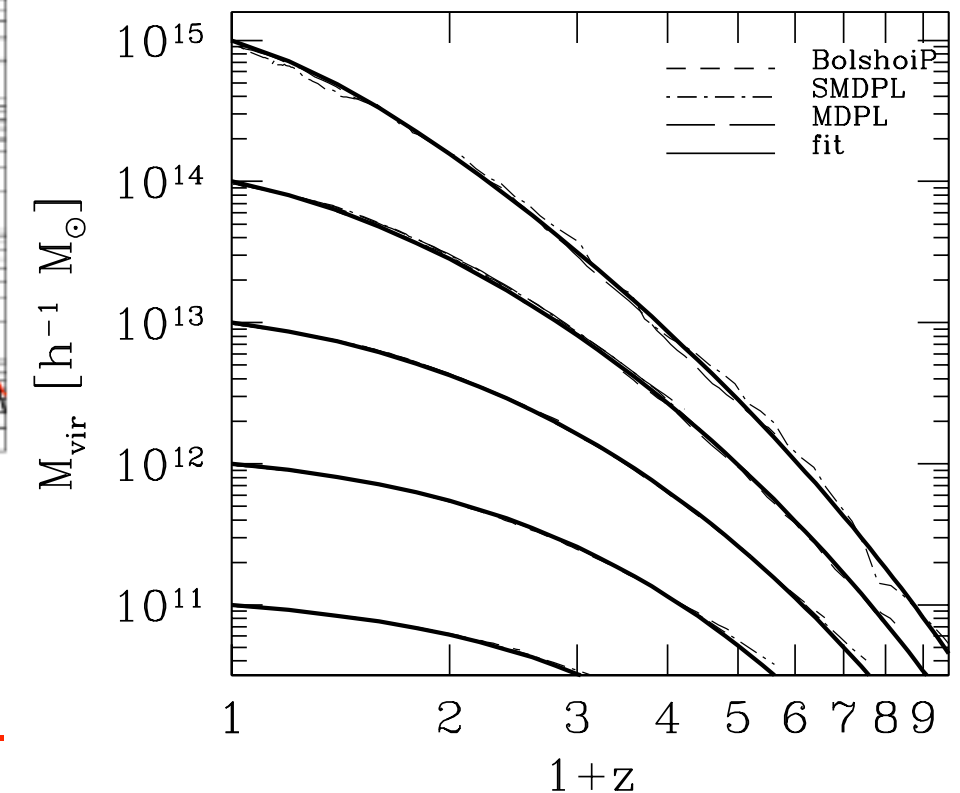


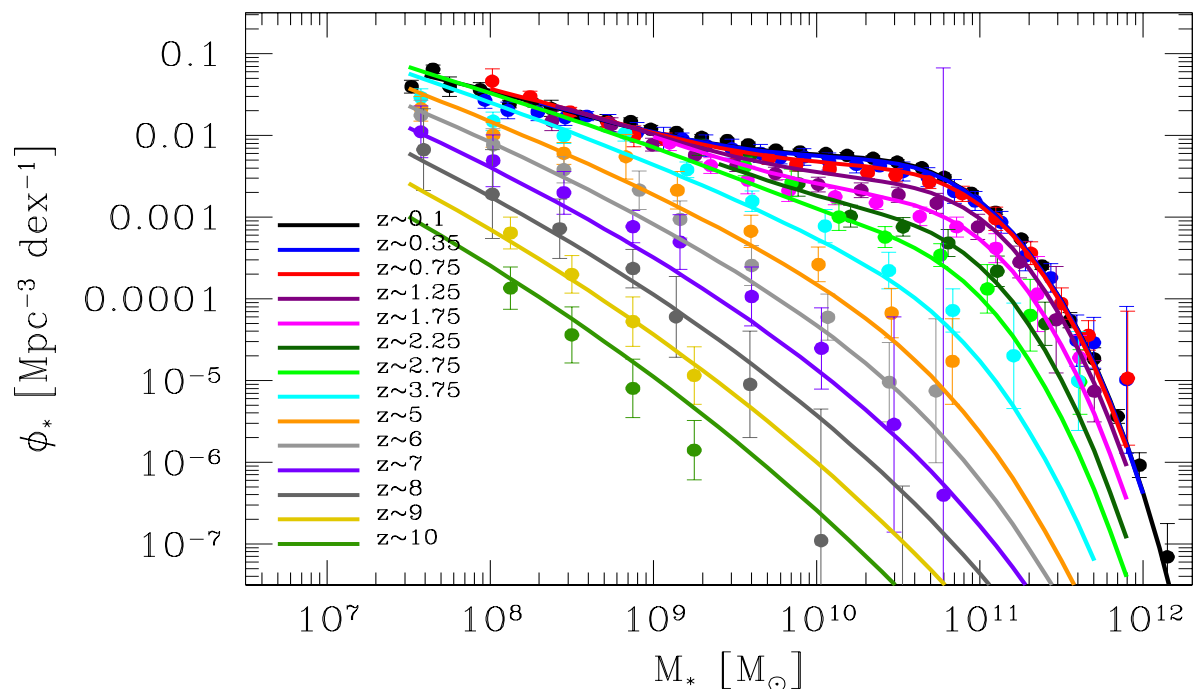
**Figure B2.** Median halo mass growth for progenitors  $z = 0$  with masses of  $M_{\text{vir}} = 10^{11}, 10^{12}, 10^{13}, 10^{14}$  and  $10^{15} h^{-1} M_{\odot}$ , solid lines. Fits to simulations are shown with the dotted lines.

# Constraining the Galaxy Halo Connection: Star Formation Histories, Galaxy Mergers, and Structural Properties, by Aldo Rodriguez-Puebla, Joel Primack, Vladimir Avila-Reese, and Sandra Faber

**Table 1.** Observational data on the galaxy stellar mass function

Author	Redshift <sup>a</sup>	$\Omega$ [deg <sup>2</sup> ]	Corrections
Bell et al. (2003)	$z \sim 0.1$	462	I+SP+C
Yang, Mo & van den Bosch (2009a)	$z \sim 0.1$	4681	I+SP+C
Li & White (2009)	$z \sim 0.1$	6437	I+P+C
Bernardi et al. (2010)	$z \sim 0.1$	4681	I+SP+C
Bernardi et al. (2013)	$z \sim 0.1$	7748	I+SP+C
Rodriguez-Puebla et al. in prep	$z \sim 0.1$	7748	S
Drory et al. (2009)	$0 < z < 1$	1.73	SP+C
Moustakas et al. (2013)	$0 < z < 1$	9	SP+D+C
Pérez-González et al. (2008)	$0.2 < z < 2.5$	0.184	I+SP+D+C
Tomczak et al. (2014)	$0.2 < z < 3$	0.0878	C
Ilbert et al. (2013)	$0.2 < z < 4$	2	C
Muzzin et al. (2013)	$0.2 < z < 4$	1.62	I+C
Santini et al. (2012)	$0.6 < z < 4.5$	0.0319	I+C
Mortlock et al. (2011)	$1 < z < 3.5$	0.0125	I+C
Marchesini et al. (2009)	$1.3 < z < 4$	0.142	I+C
Stark et al. (2009)	$z \sim 6$	0.089	I
Lee et al. (2012)	$3 < z < 7$	0.089	I+SP+C
González et al. (2011)	$4 < z < 7$	0.0778	I+C
Duncan et al. (2014)	$4 < z < 7$	0.0778	C
Song et al. (2015)	$4 < z < 8$	0.0778	I
This paper, Appendix D	$4 < z < 10$	0.0778	-

I=IMF; P= photometry corrections; S=Surface Brightness correction; D=Dust model;  
NE= Nebular Emissions; SP = SPS Model; C = Cosmology

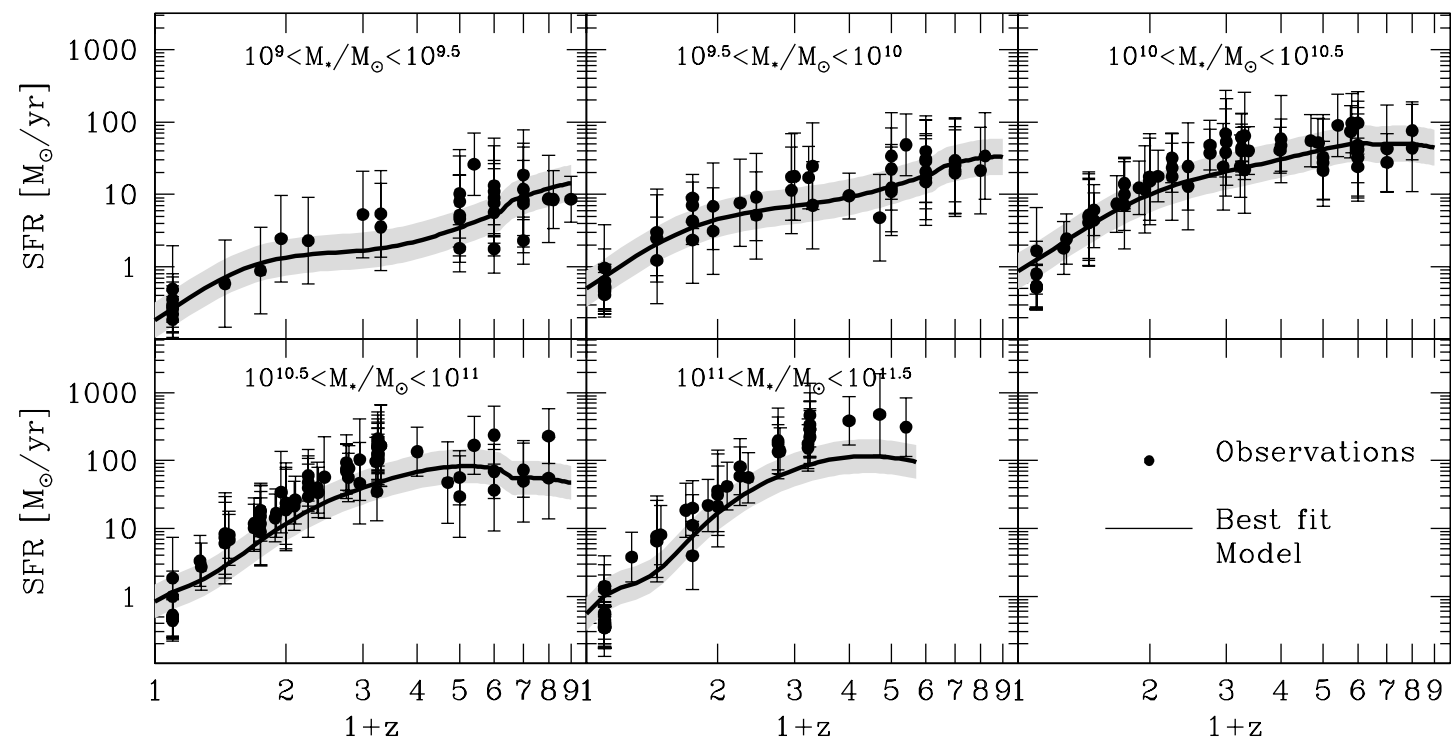


**Redshift evolution from  $z \sim 0.1$  to  $z \sim 10$  of the galaxy stellar mass function (GSMF) derived by using 20 observational samples from the literature and represented with the filled circles with error bars. The various GSMFs have been homogenized and corrected for potential systematics that could affect our results, see the text for details. Solid lines are the best fit model from a set of  $3 \times 10^5$  MCMC trials.**

**Table 2.** Observational data on the star formation rates

Author	Redshift <sup>a</sup>	SFR Estimator	Corrections	Type
Chen et al. (2009)	$z \sim 0.1$	$H_\alpha/H_\beta$	S	All
Salim et al. (2007)	$z \sim 0.1$	UV SED	S	All
Noeske et al. (2007)	$0.2 < z < 1.1$	UV+IR	S	All
Karim et al. (2011)	$0.2 < z < 3$	1.4 GHz	I+S+E	All
Dunne et al. (2009)	$0.45 < z < 2$	1.4 GHz	I+S+E	All
Kajisawa et al. (2010)	$0.5 < z < 3.5$	UV+IR	I	All
Whitaker et al. (2014)	$0.5 < z < 3$	UV+IR	I+S	All
Sobral et al. (2014)	$z \sim 2.23$	$H_\alpha$	I+S+SP	SF
Reddy et al. (2012)	$2.3 < z < 3.7$	UV+IR	I+S+SP	SF
Magdis et al. (2010)	$z \sim 3$	FUV	I+S+SP	SF
Lee et al. (2011)	$3.3 < z < 4.3$	FUV	I+SP	SF
Lee et al. (2012)	$3.9 < z < 5$	FUV	I+SP	SF
González et al. (2012)	$4 < z < 6$	UV+IR	I+NE	SF
Salmon et al. (2015)	$4 < z < 6$	UV SED	I+NE+E	SF
Bouwens et al. (2011)	$4 < z < 7.2$	FUV	I+S	SF
Duncan et al. (2014)	$4 < z < 7$	UV SED	I+NE	SF
Shim et al. (2011)	$z \sim 4.4$	$H_\alpha$	I+S+SP	SF
Steinhardt et al. (2014)	$z \sim 5$	UV SED	I+S	SF
González et al. (2010)	$z = 7.2$	UV+IR	I+NE	SF
This paper, Appendix D	$4 < z < 8$	FUV	I+E+NE	SF

I=IMF; S=Star formation calibration; E=Extinction; NE= Nebular Emissions; SP=SPS Model



**Star formation rates as a function of redshift  $z$  in five stellar mass bins. Black solid lines shows the resulting best fit model to the SFRs implied by our approach. The filled circles with error bars show the observed data.**

# Constraining the Galaxy Halo Connection: Star Formation Histories, Galaxy Mergers, and Structural Properties, by Aldo Rodriguez-Puebla, Joel Primack, Vladimir Avila-Reese, and Sandra Faber

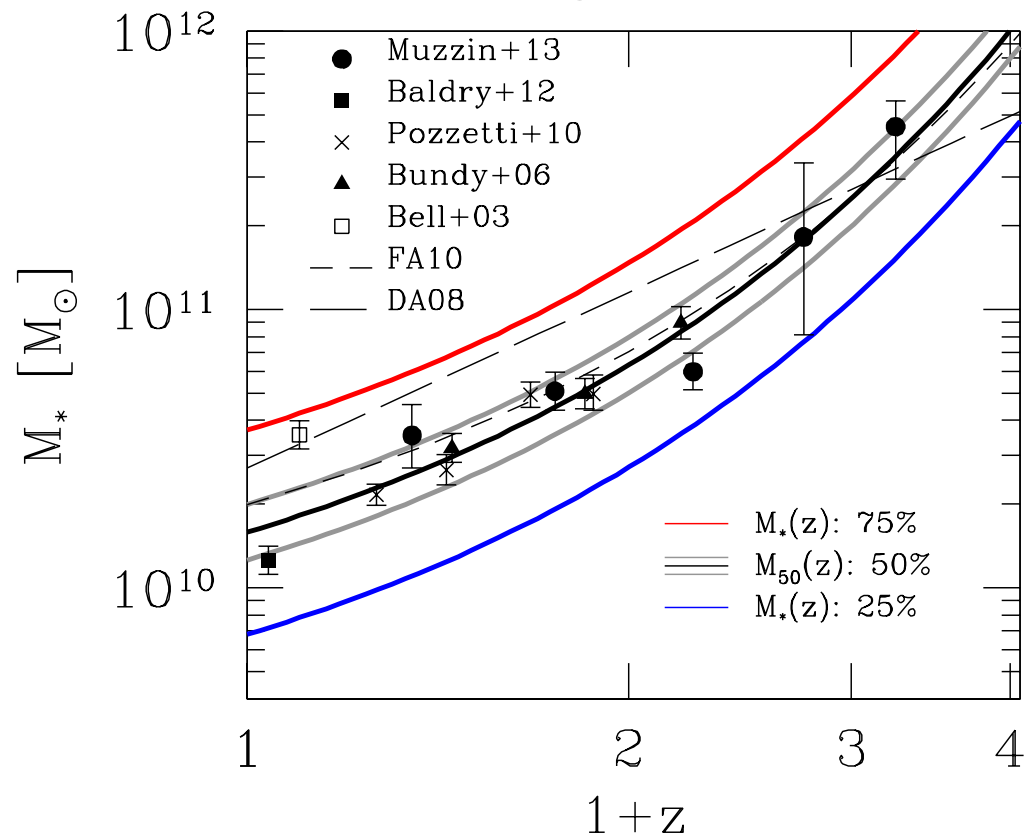


**Figure 1.** The stellar mass  $M_{50}(z)$  at which the fractions of blue star-forming and red quenched galaxies are both 50%. The open square with error bars shows the transition mass for local galaxies as derived in Bell et al. (2003) based on the SDSS DR2 and using the  $g - r$  color magnitude diagram, while the filled triangles show the transition mass derived in Bundy et al. (2006) based on the DEEP2 survey and using the  $U - B$  color magnitude diagram. The long dashed line shows the results of Drory & Alvarez (2008) based on the FORS Deep Field survey using the SFR distribution. The x symbols show observations from Pozzetti et al. (2010) based on the COSMOS survey using the SFR distribution. A filled square shows observations from Baldry et al. (2012) based on the GAMA survey using the  $g - r$  color magnitude diagram. Filled circles show observations from Muzzin et al. (2013) based on the COSMOS/ULTRAVISTA survey using the UVJ diagram. The short dashed line shows the empirical results based on abundance matching and using the SFR distribution by Firmani & Avila-Reese (2010). The solid black line shows the relation  $\log(M_{50}(z)/M_{\odot}) = 10.2 + 0.6z$  employed in this paper, which is consistent with most of the above studies. The gray solid lines show the results when shifting  $(M_{50}(z)/M_{\odot})$  0.1 dex higher and lower. The red (blue) curves show the stellar mass vs.  $z$  where 75% (25%) of the galaxies are quenched.

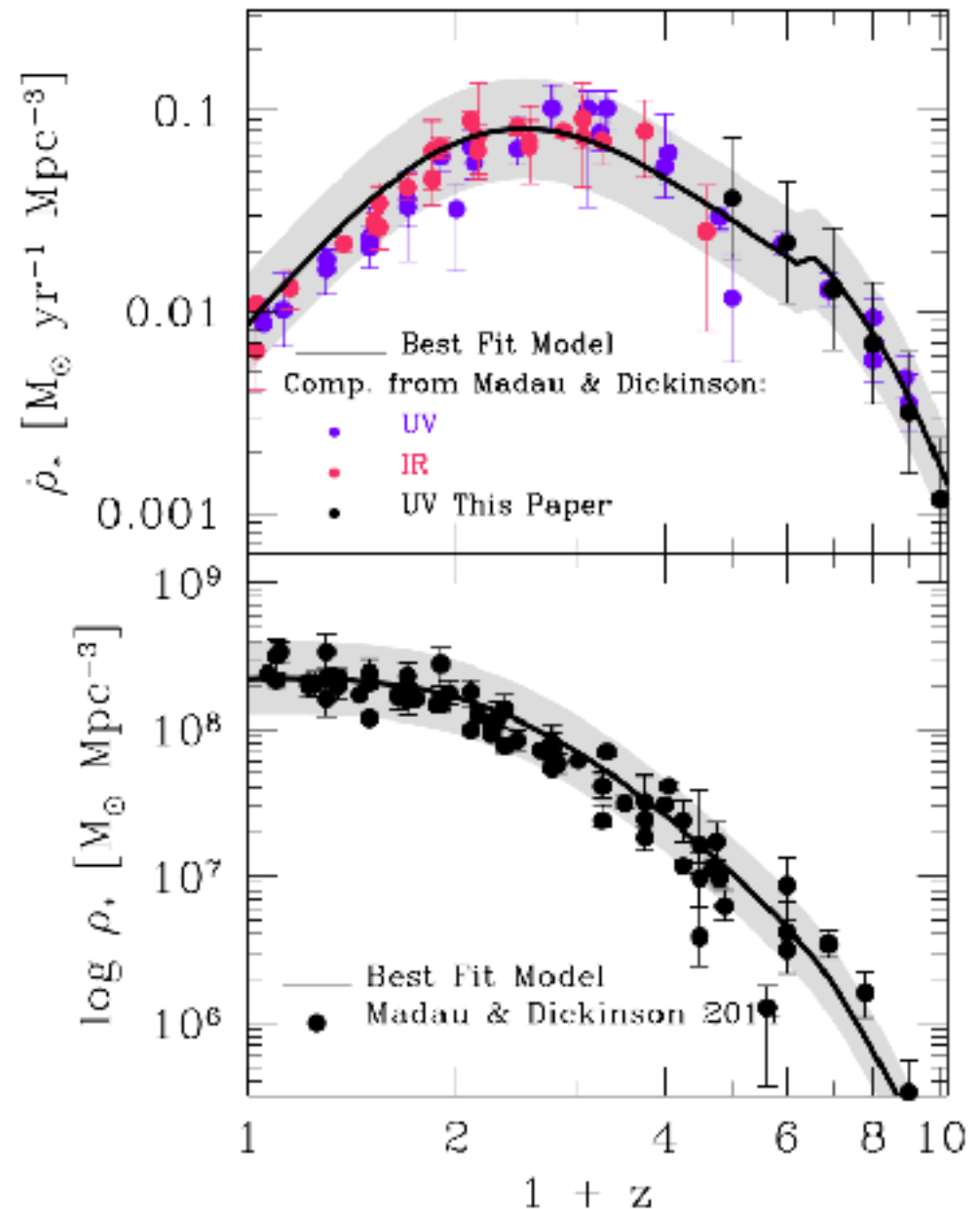
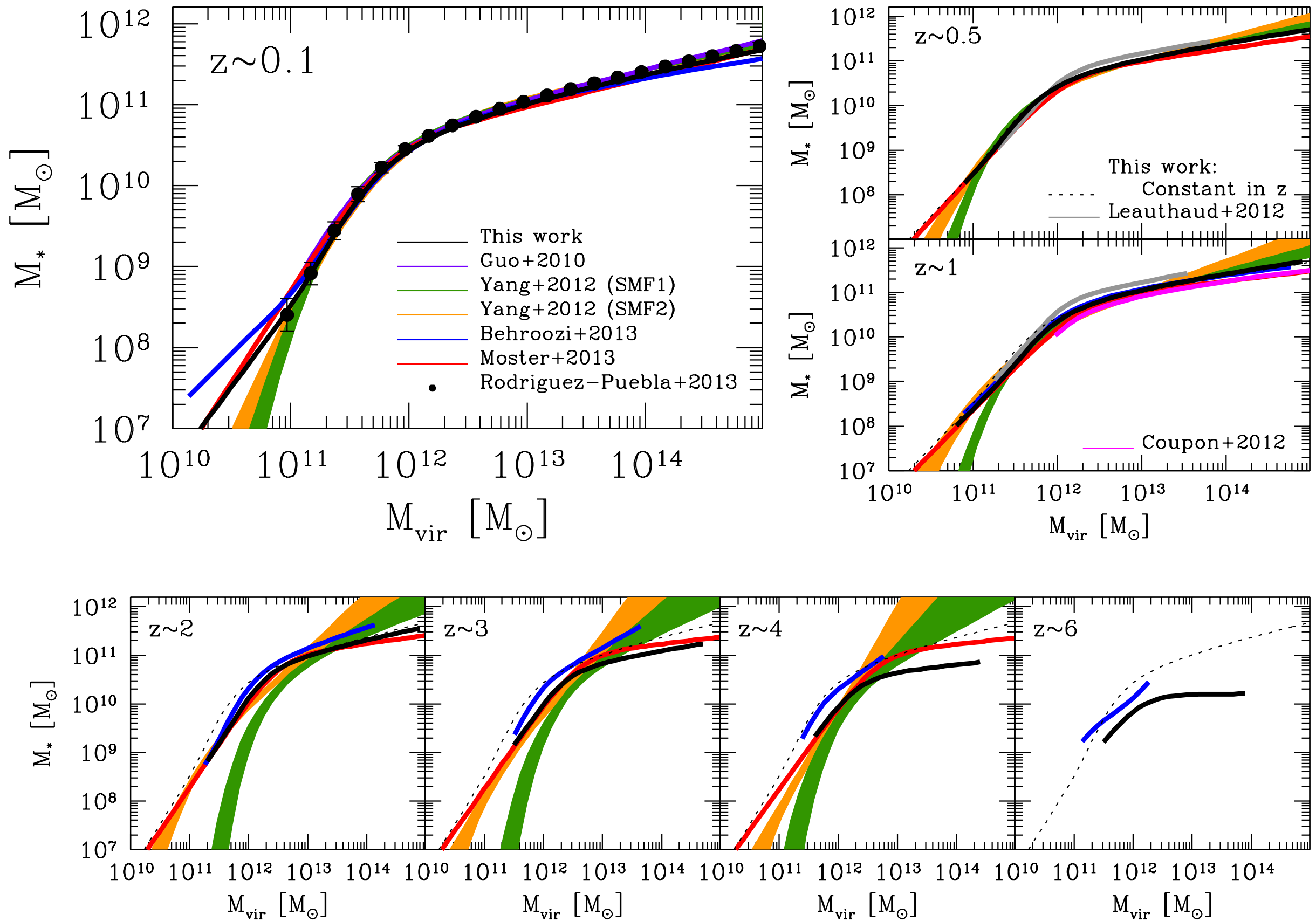
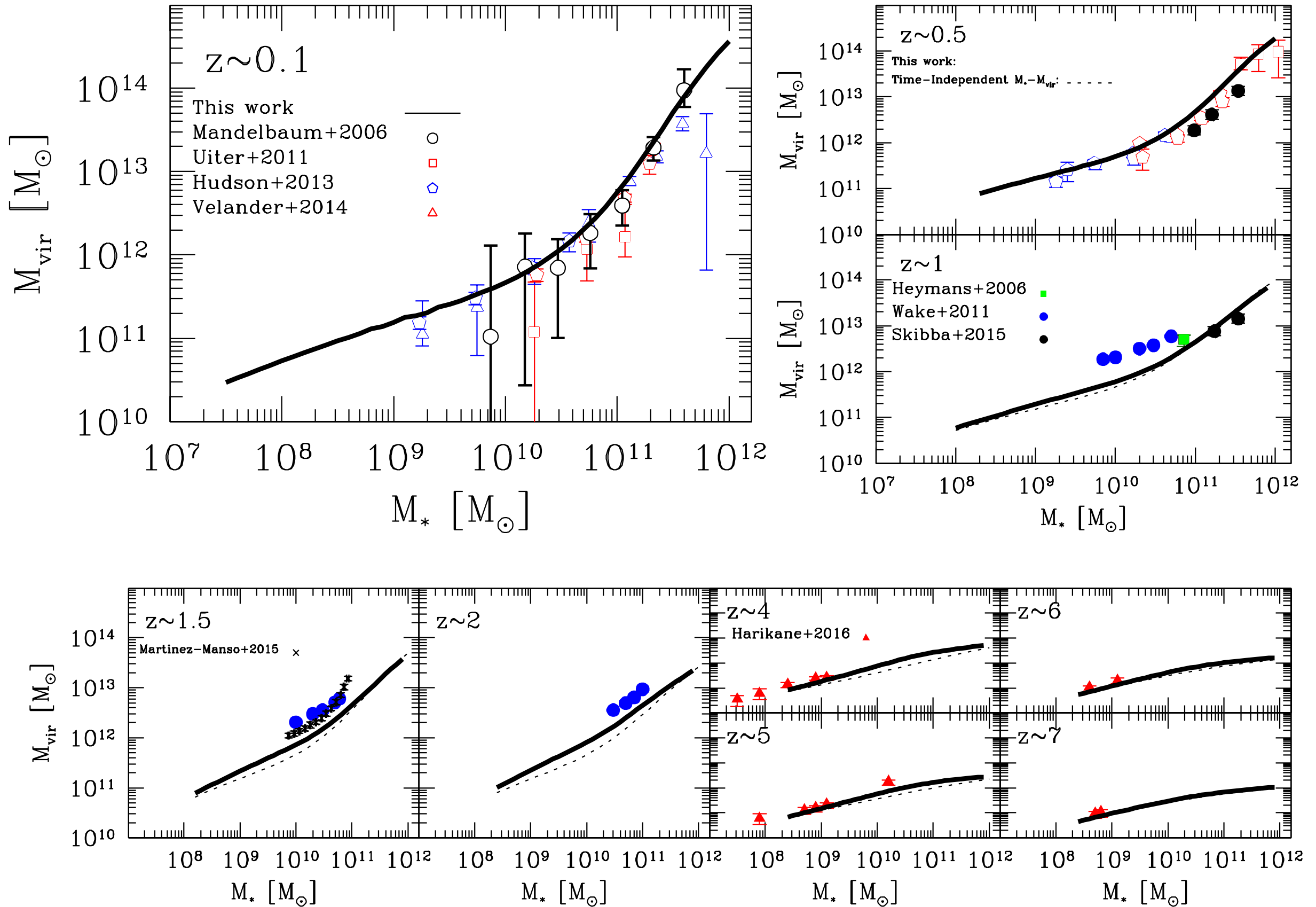


**Figure 5. Upper Panel:** Cosmic star formation rate, CSFR. The solid black line shows the resulting best fit model to the CSFR as described in Section 2.4. Filled red and violet circles show a set of compiled observations by Madau & Dickinson (2014) from FUV+IR rest frame luminosities. UV luminosities are dust-corrected. Black solid circles show the results from the UV dust-corrected luminosity functions described in Appendix D. **Lower Panel:** Cosmic stellar mass density. The solid black line shows the predictions for our best fit model. Filled black circles show the data points compiled in Madau & Dickinson (2014). All data was adjusted to the IMF of Chabrier (2003). In both panels, the light grey shaded area shows the systematic assumed to be of 0.25 dex.

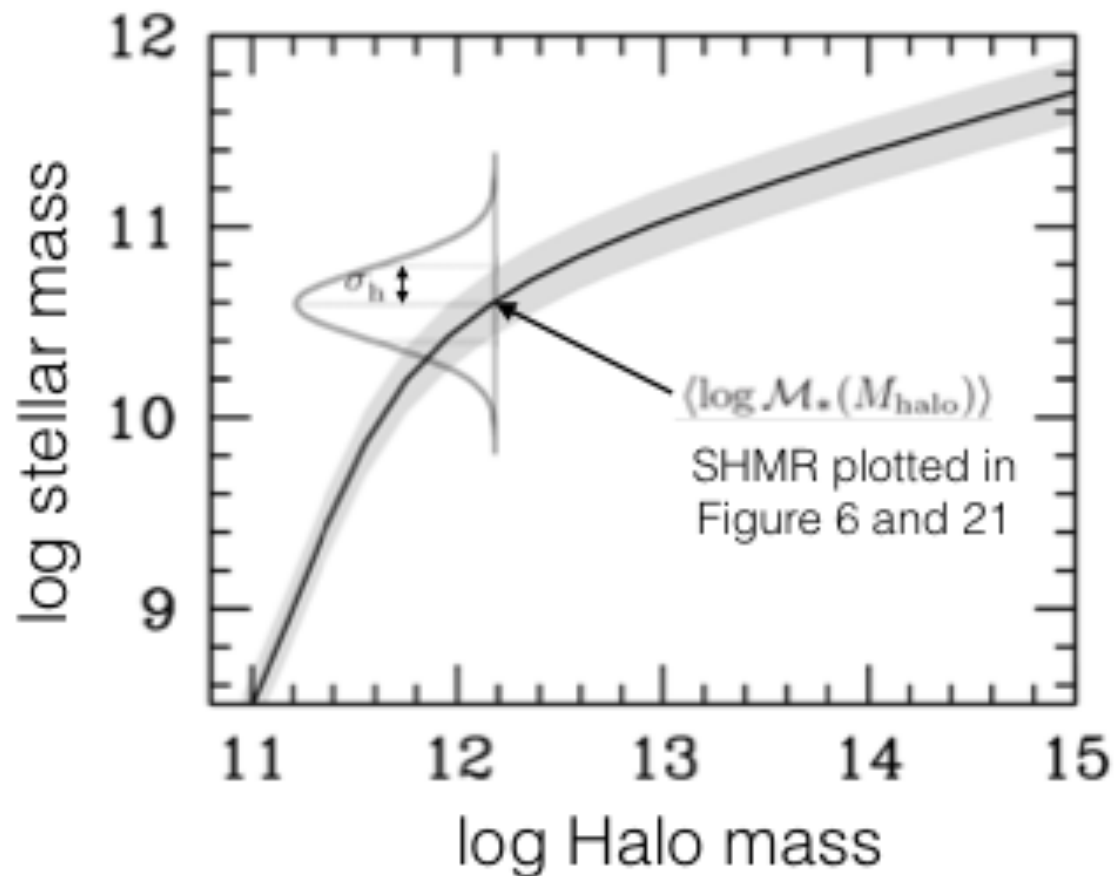
# Constraining the Galaxy Halo Connection: Star Formation Histories, Galaxy Mergers, and Structural Properties, by Aldo Rodriguez-Puebla, Joel Primack, Vladimir Avila-Reese, and Sandra Faber



# Constraining the Galaxy Halo Connection: Star Formation Histories, Galaxy Mergers, and Structural Properties, by Aldo Rodriguez-Puebla, Joel Primack, Vladimir Avila-Reese, and Sandra Faber



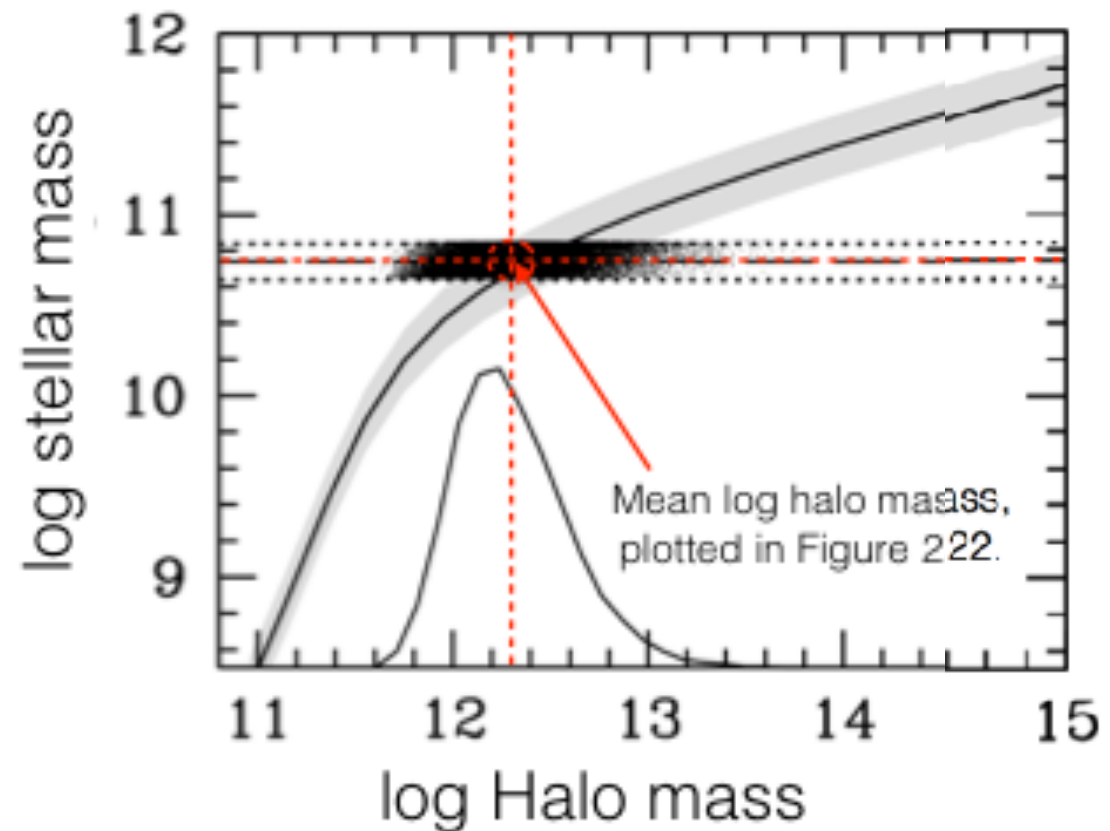
## Distributions at a fixed Halo Mass: Assumption in SHAM



$$\mathcal{H}(M_* | M_{\text{halo}}) = \frac{1}{\sqrt{2\pi\sigma_h^2}} \exp \left[ -\frac{(\log M_* - \langle \log \mathcal{M}_*(M_{\text{halo}}) \rangle)^2}{2\sigma_h^2} \right]$$

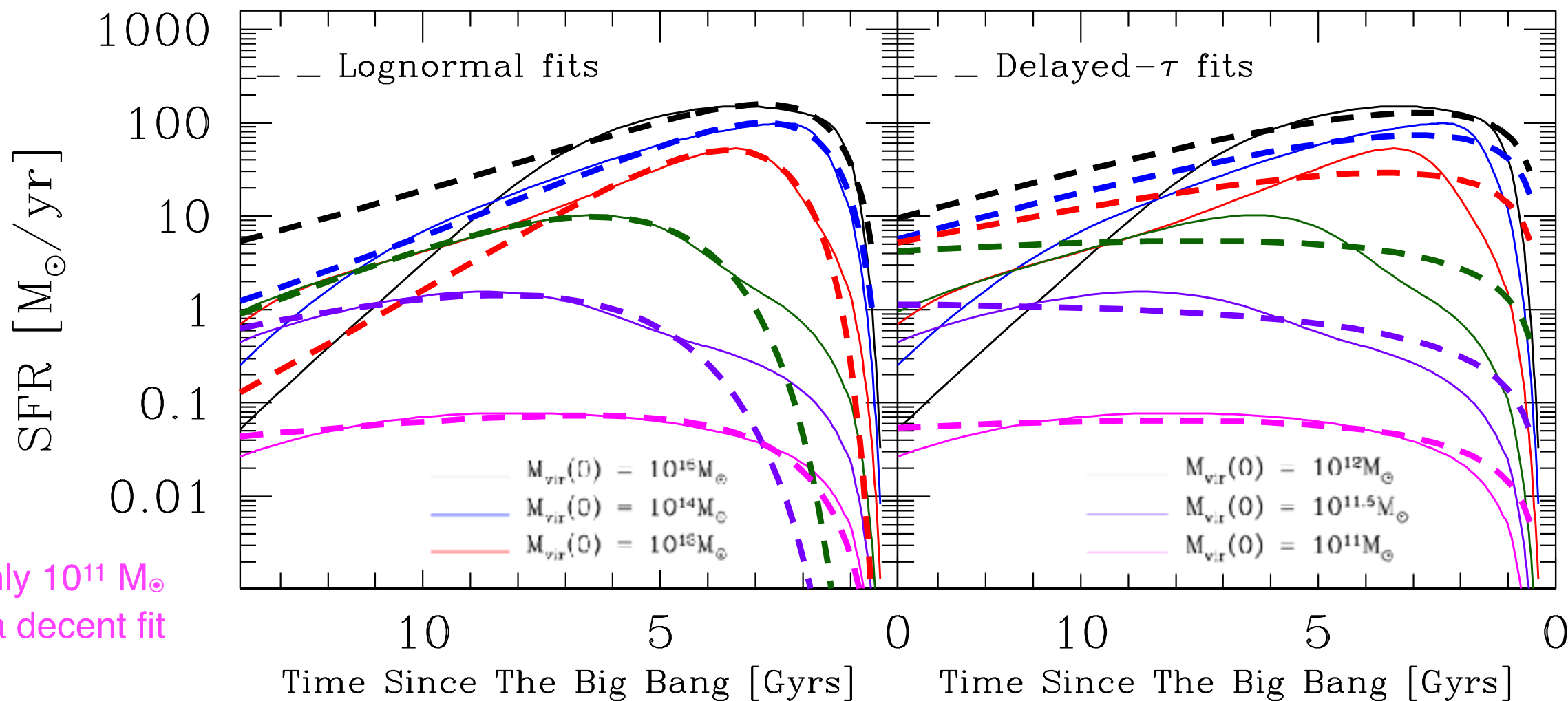
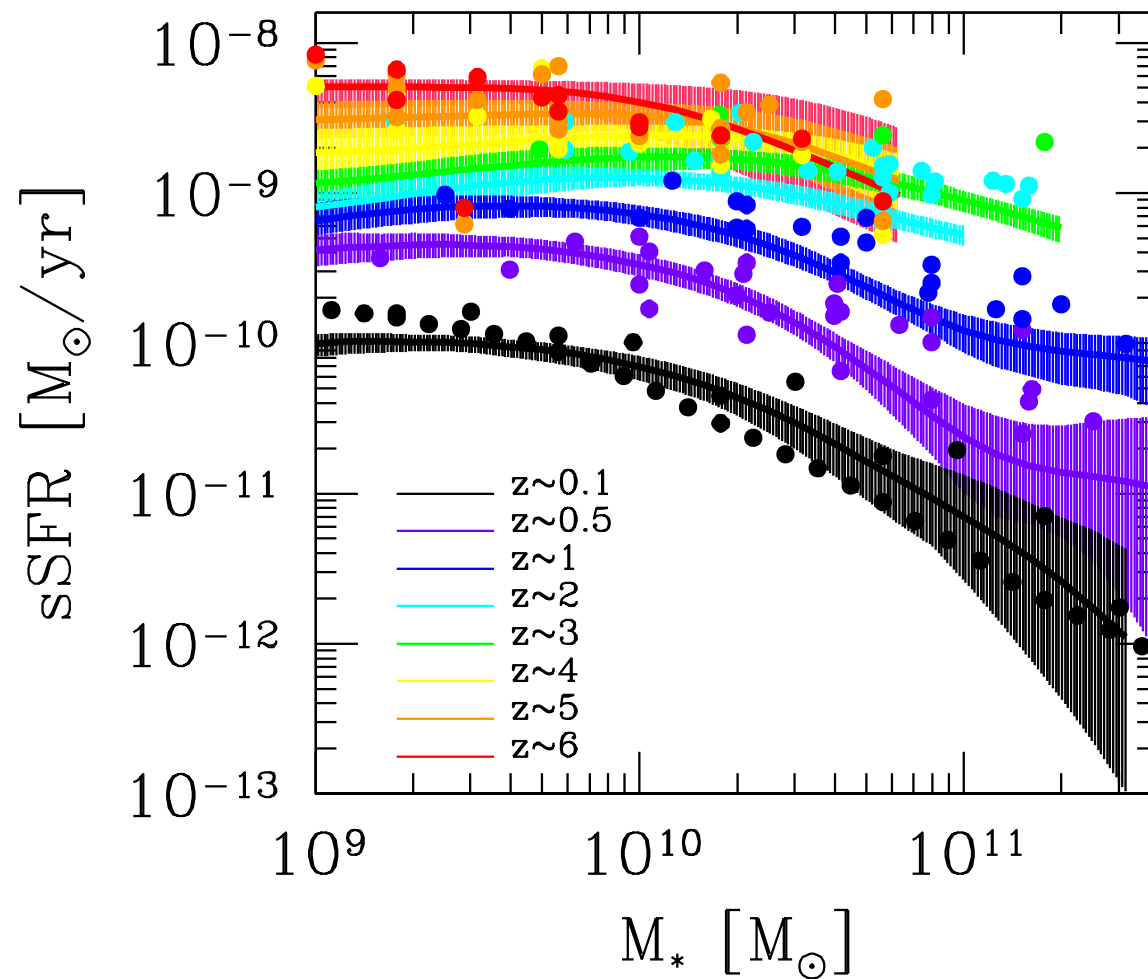
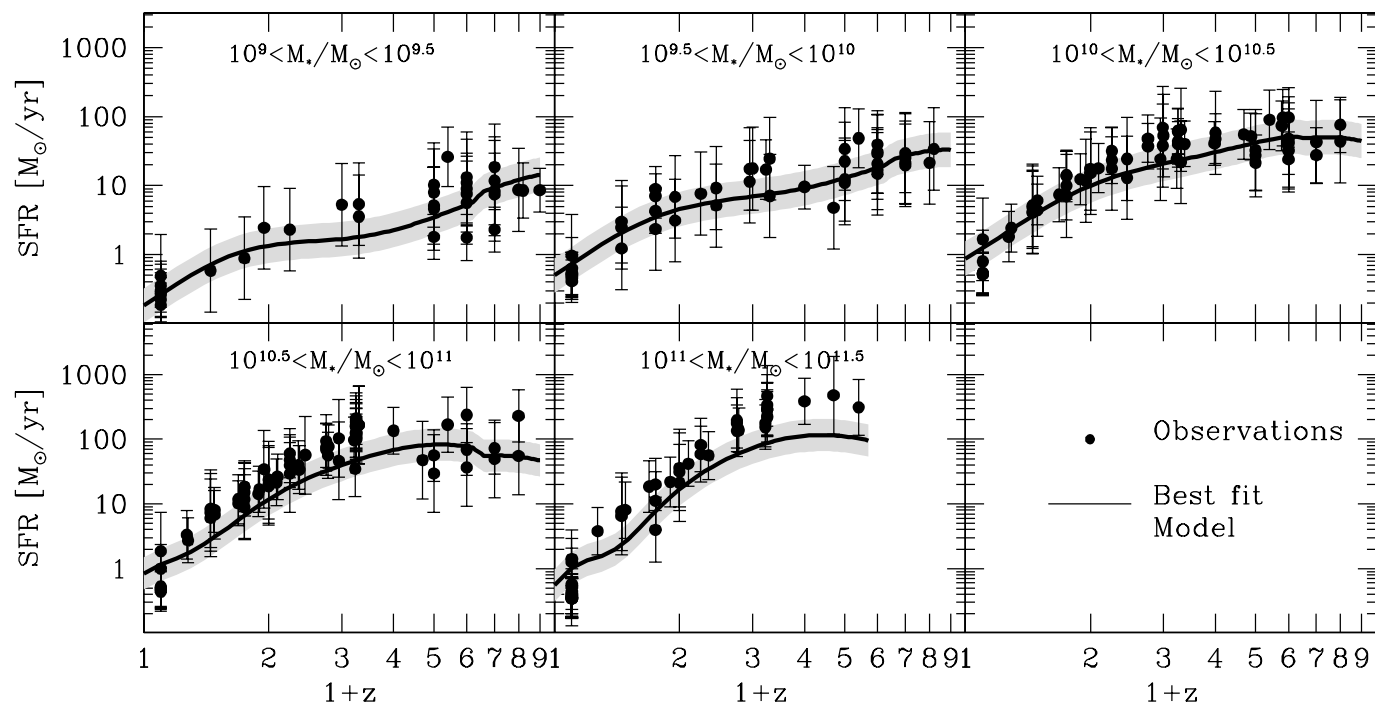
Galaxies are randomly distributed around the mean relation (solid black line,  $\langle \log \mathcal{M}_*(M_{\text{halo}}) \rangle$ ) by following a gaussian distribution with dispersion  $\sigma_h$

## Distributions at a fixed Stellar Mass: Observational papers that select stellar mass bins/thresholds

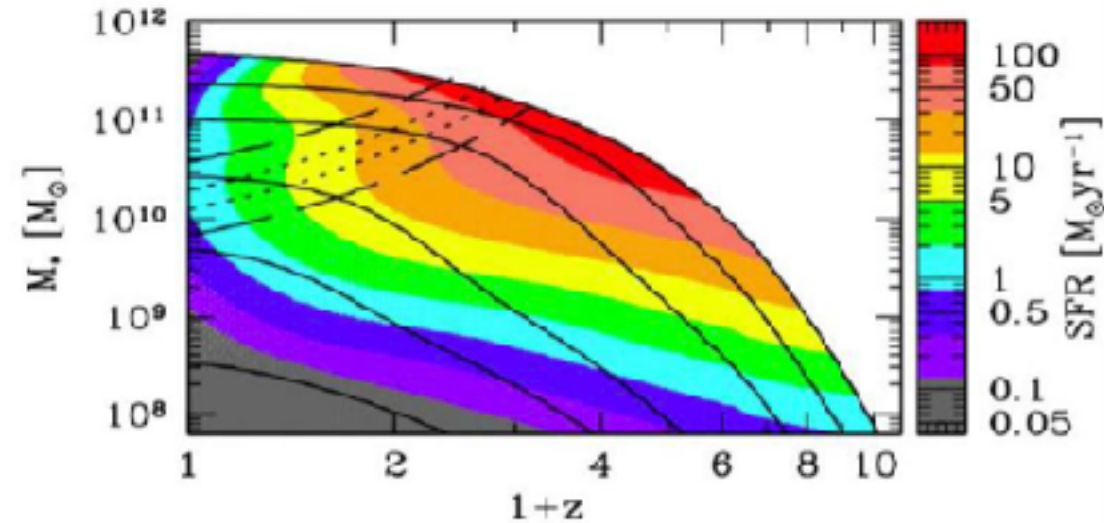
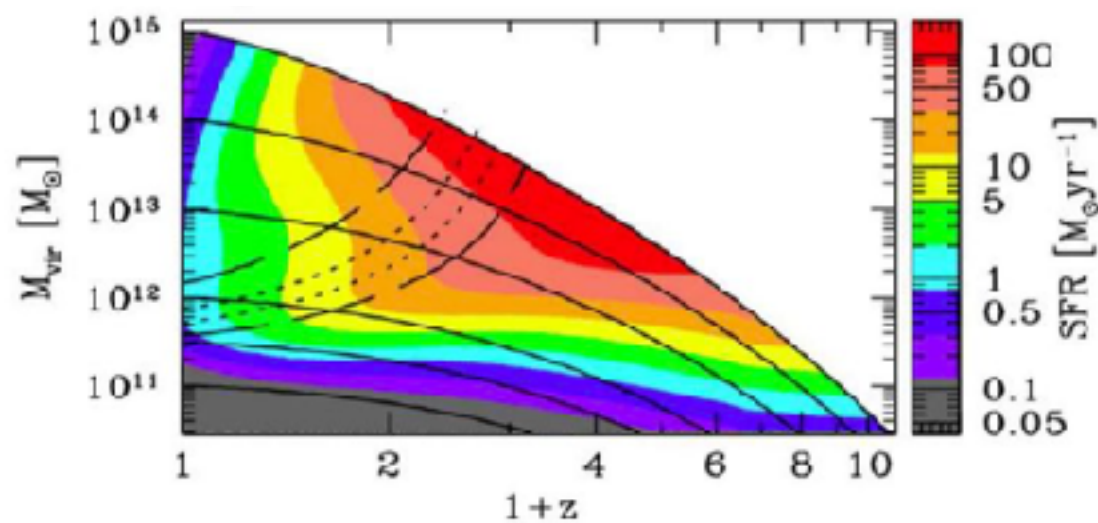
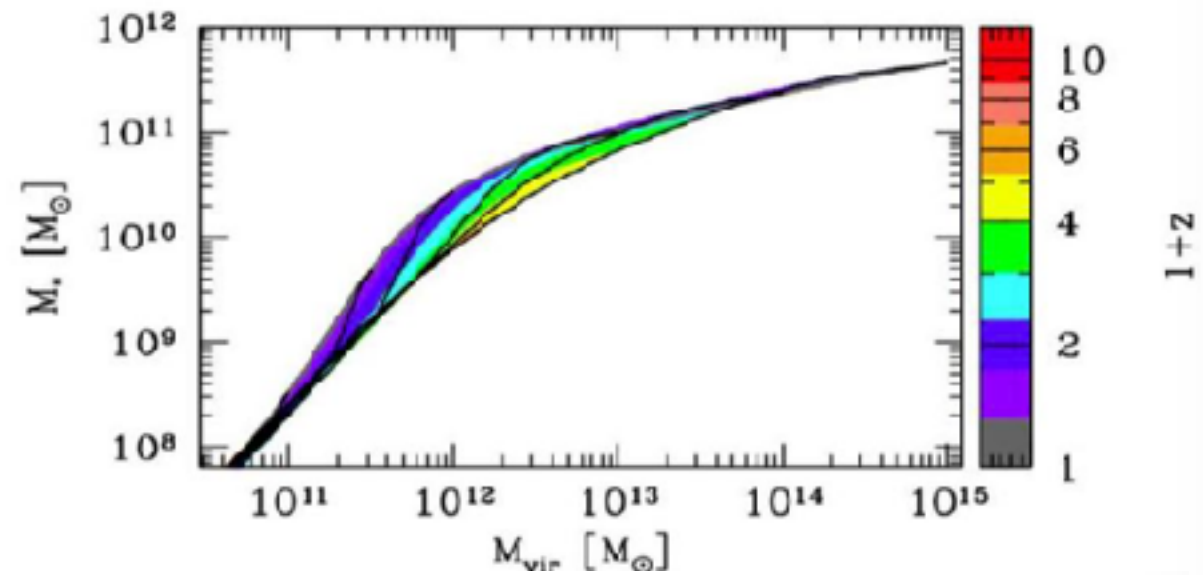
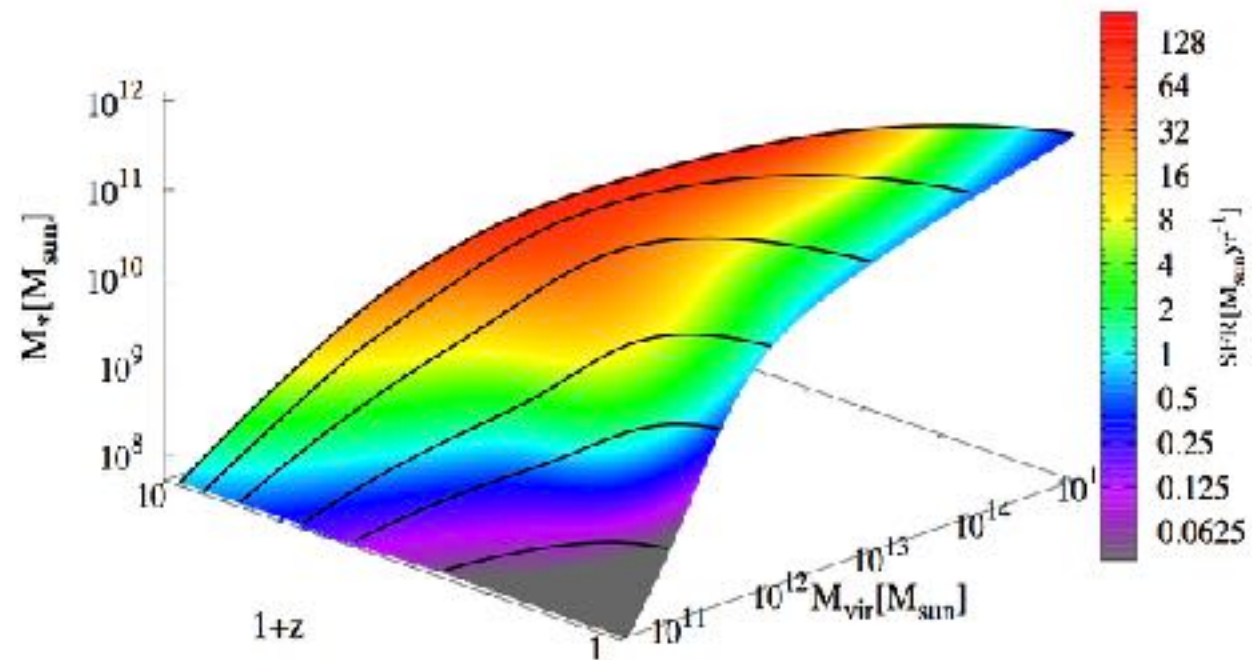


When selecting galaxies at a fixed  $M_*$ , the points are not longer distributed as Gaussians. The mean log halo mass is not longer located in the solid black line but is slightly shifted towards low halo masses. This is more dramatic at high masses. The reason is that the distribution of points at a fixed stellar mass depends on the number density of galaxies and halos.

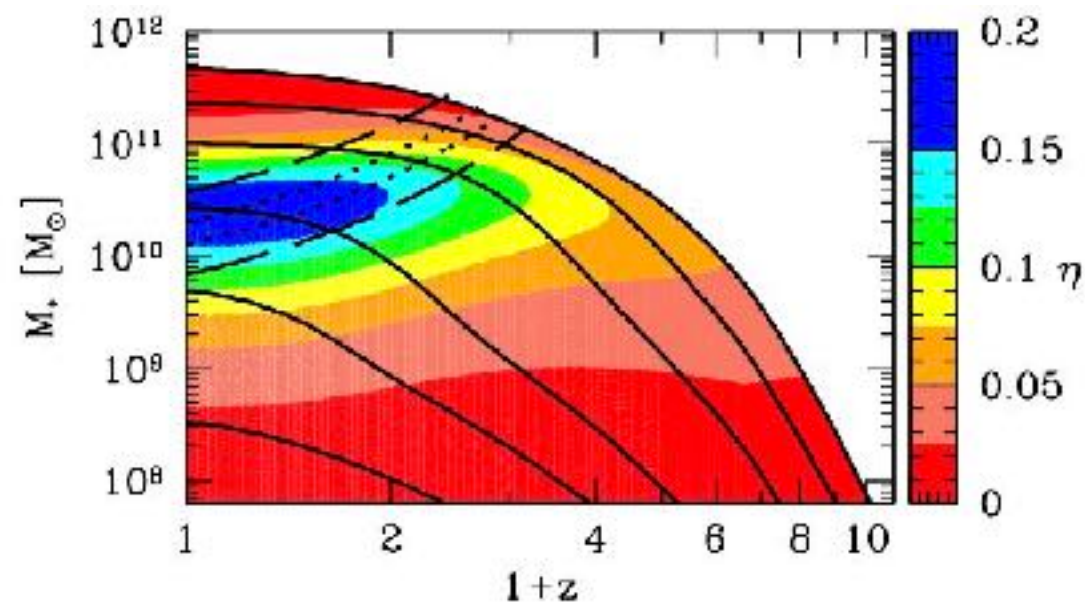
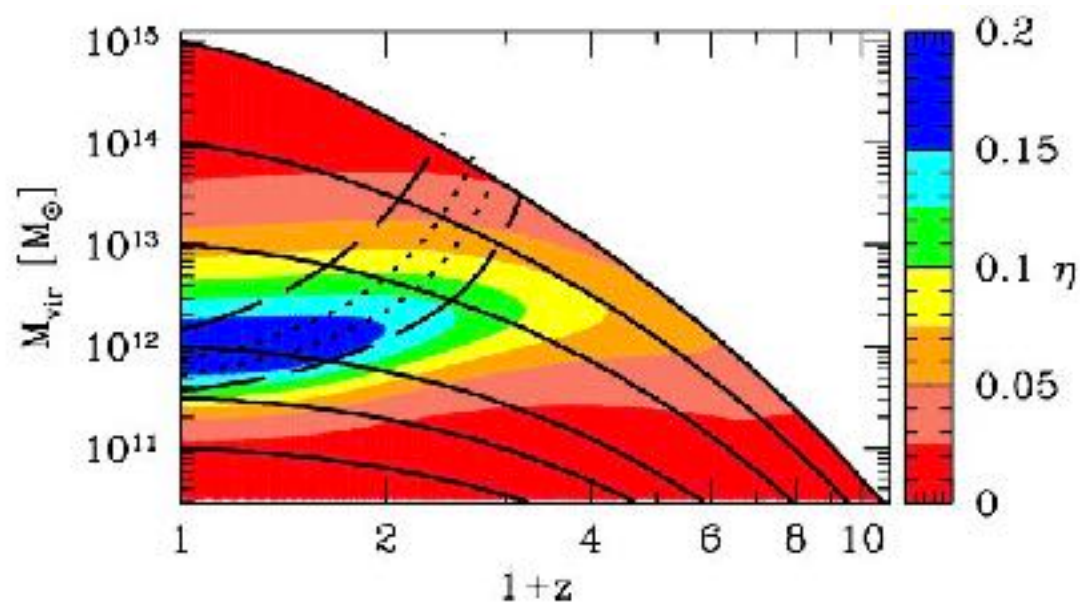
# SFR DATA & FITS



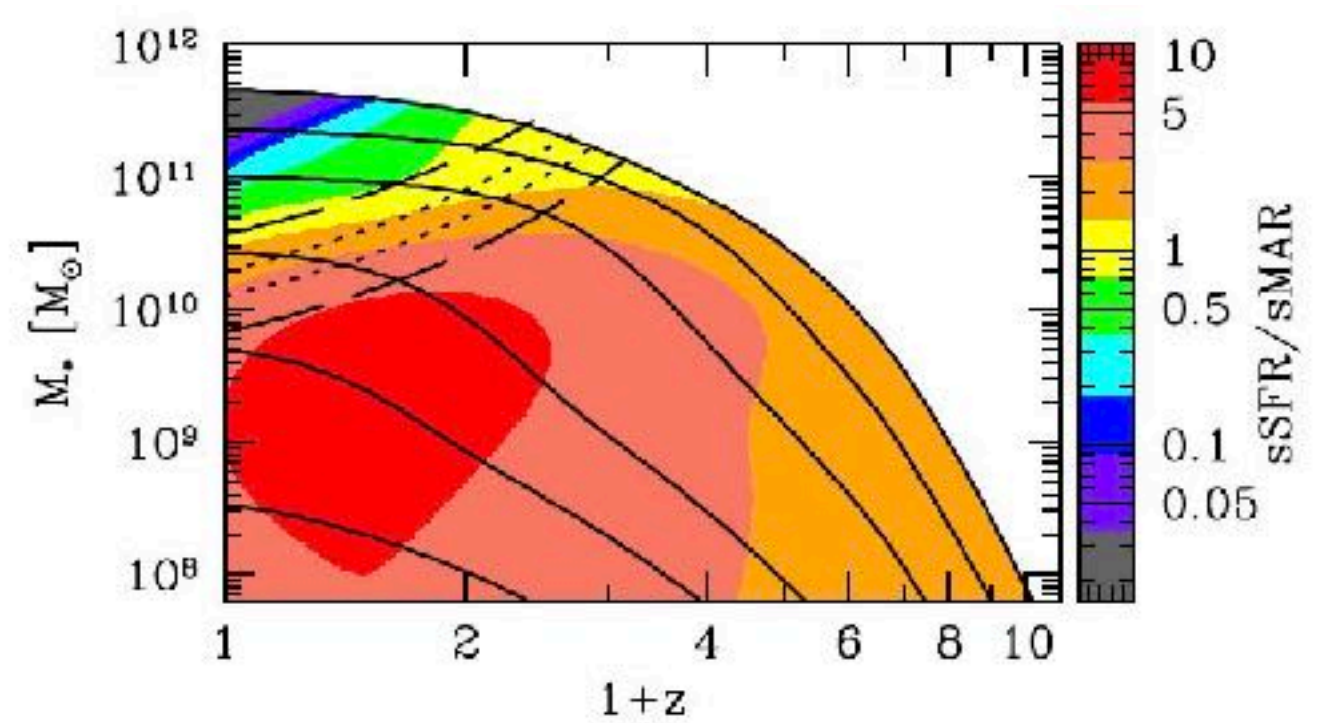
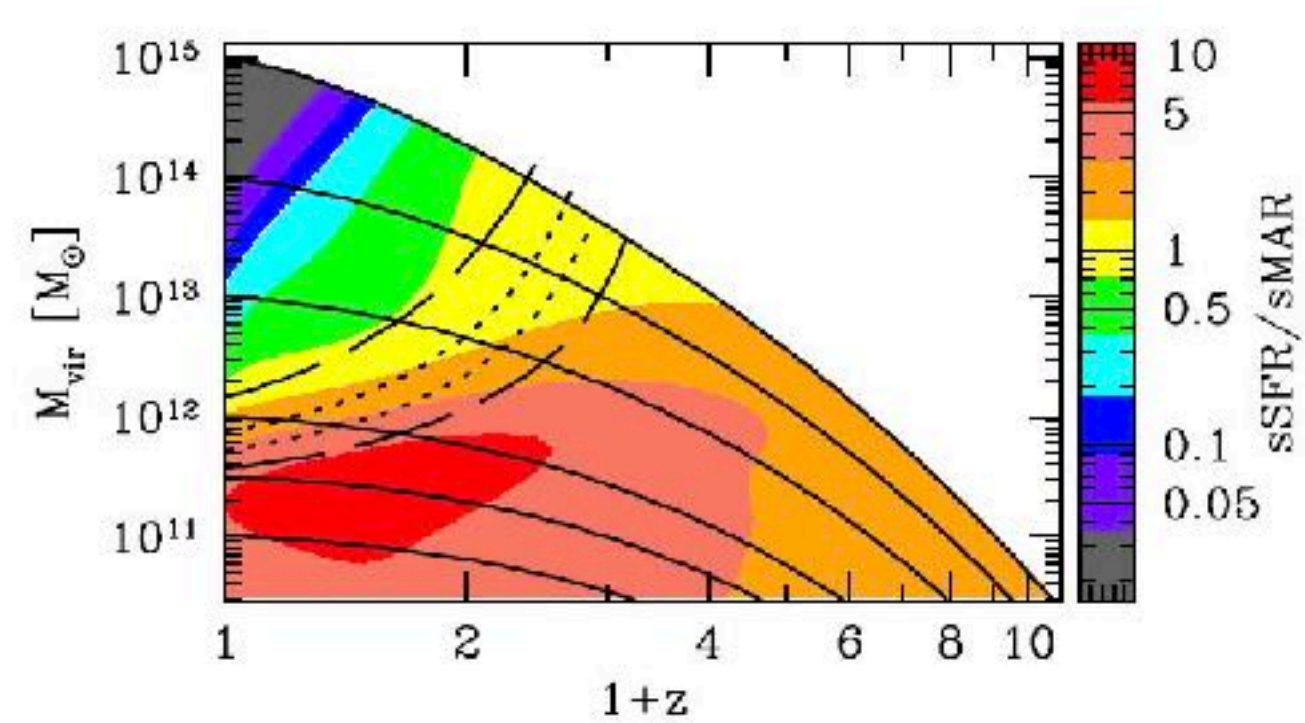
Only  $10^{11} M_{\odot}$  is a decent fit



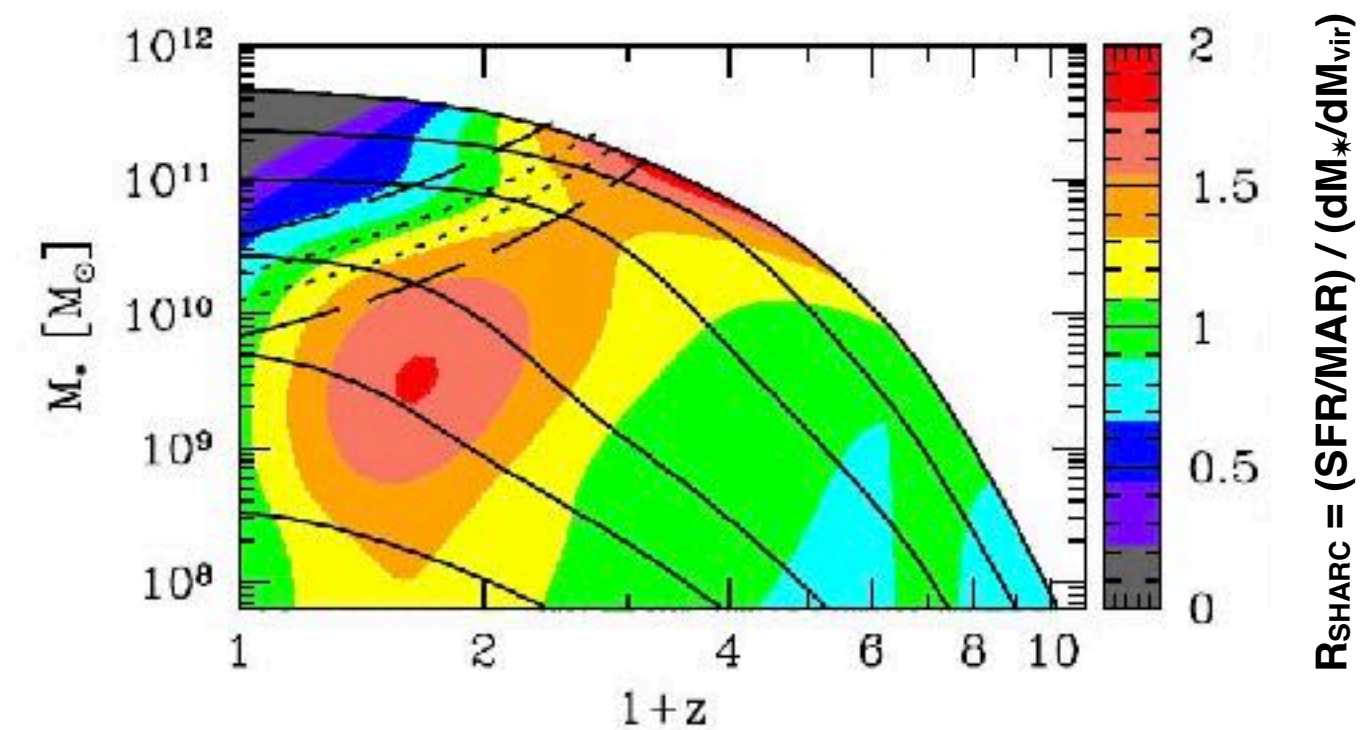
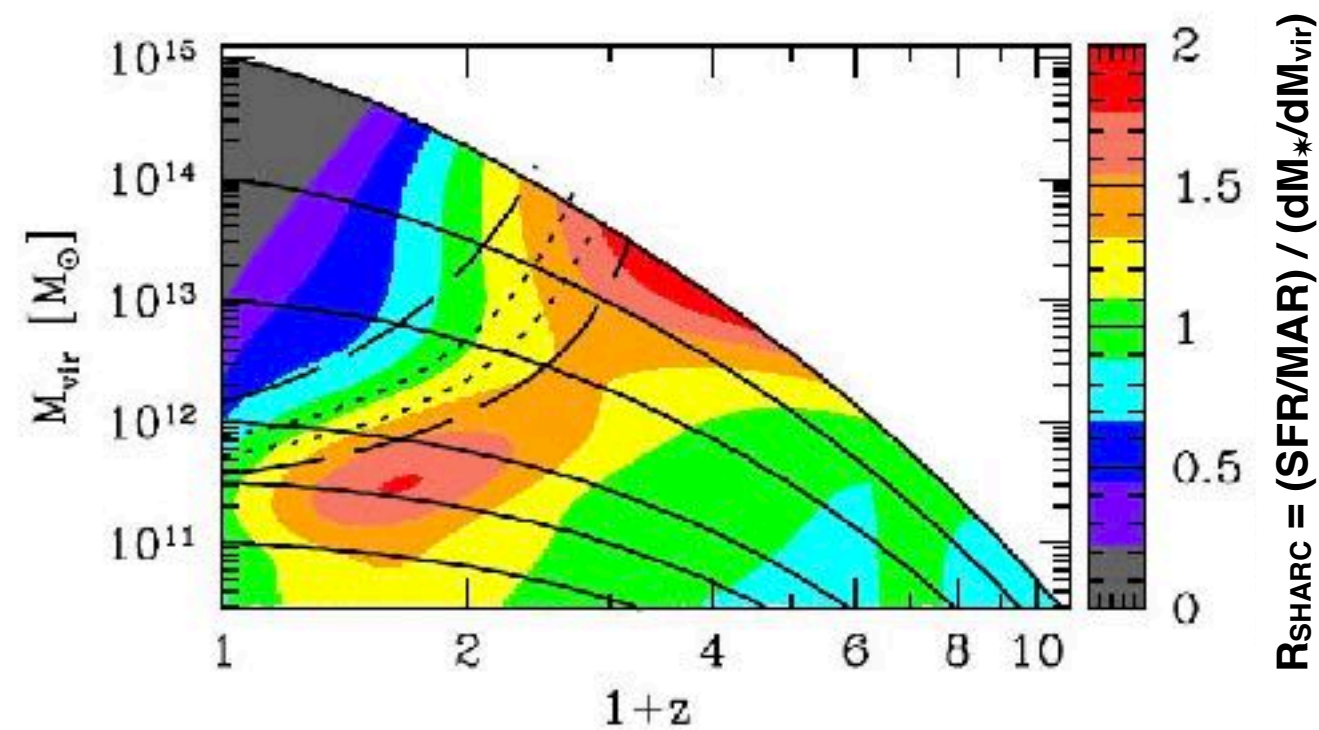
The star formation rate (SFR) as a function of redshift and (left panel)  $M_{\text{vir}}$  and (right panel)  $M_*$



The integral stellar conversion  $\eta = f_*/f_b$ , where  $f_* = M_*/M_{\text{vir}}$  and  $f_b = \Omega_B/\Omega_M$



This figure shows that quenching is correlated with  $s\text{SFR}/s\text{SMR} = t_{\text{halo}}/t_*$ , since  $s\text{SFR}/s\text{SMR}$  and quenching curves are nearly parallel.  $s\text{SFR}/s\text{SMR}$  - first rises, reaching a peak  $\sim 2$  at  $z \sim 3$  for  $10^{13}$  halos, a peak  $\sim 7$  for  $10^{12}$  halos at  $z \sim 1.5$ , and  $10^{11}$  halos are still at peak  $s\text{SFR}/s\text{SMR} \sim 10$  - then declines along all  $M_{\text{vir}}$  and  $M_*$  progenitor tracks toward  $z=0$ .



This figure shows that the SHARC approximation is rather well satisfied until quenching, the SHARC ratio  $R_{\text{SHARC}} = (\text{SFR} / \text{MAR}) / (dM_{\text{vir}}/d\log M^*)$  having a value of about 1 to 2 along the progenitor trajectories, and then dropping after quenching. This shows quenching is correlated with  $R_{\text{SHARC}}$  :

- the fraction of quenched galaxies is  $\sim 50\%$  when  $R_{\text{SHARC}} \sim 1$  to 1.5, and the quenched fraction is  $> 75\%$  when  $R_{\text{SHARC}}$  drops to  $\sim 1$
- like  $s\text{SFR}/s\text{SMR}$ ,  $R_{\text{SHARC}}$  first rises along all progenitor curves, reaches a peak at higher  $z$  for higher mass ( $M_{\text{vir}}$  or  $M_*$ ), and then declines
- unlike  $s\text{SFR}/s\text{SMR}$ , the peak SHARC ratio is nearly constant between 1.5 and 2 (the SHARC ratio peaks at about 2 for both  $10^{11.5}$  halos at  $z \sim 0.5$  and  $10^{15}$  halos at  $z \sim 3$ , and at about 1.5 for intermediate mass halos).

Note: the SHARC formula is  $\text{SFR} = (dM_*/dM_{\text{vir}}) \text{MAR}$  where  $\text{MAR} = dM_{\text{vir}}/dt$ . Define  $R_{\text{SHARC}} = (\text{SFR} / \text{MAR}) / (dM_*/dM_{\text{vir}})$ , so SHARC  $\implies R_{\text{SHARC}} = 1$ .

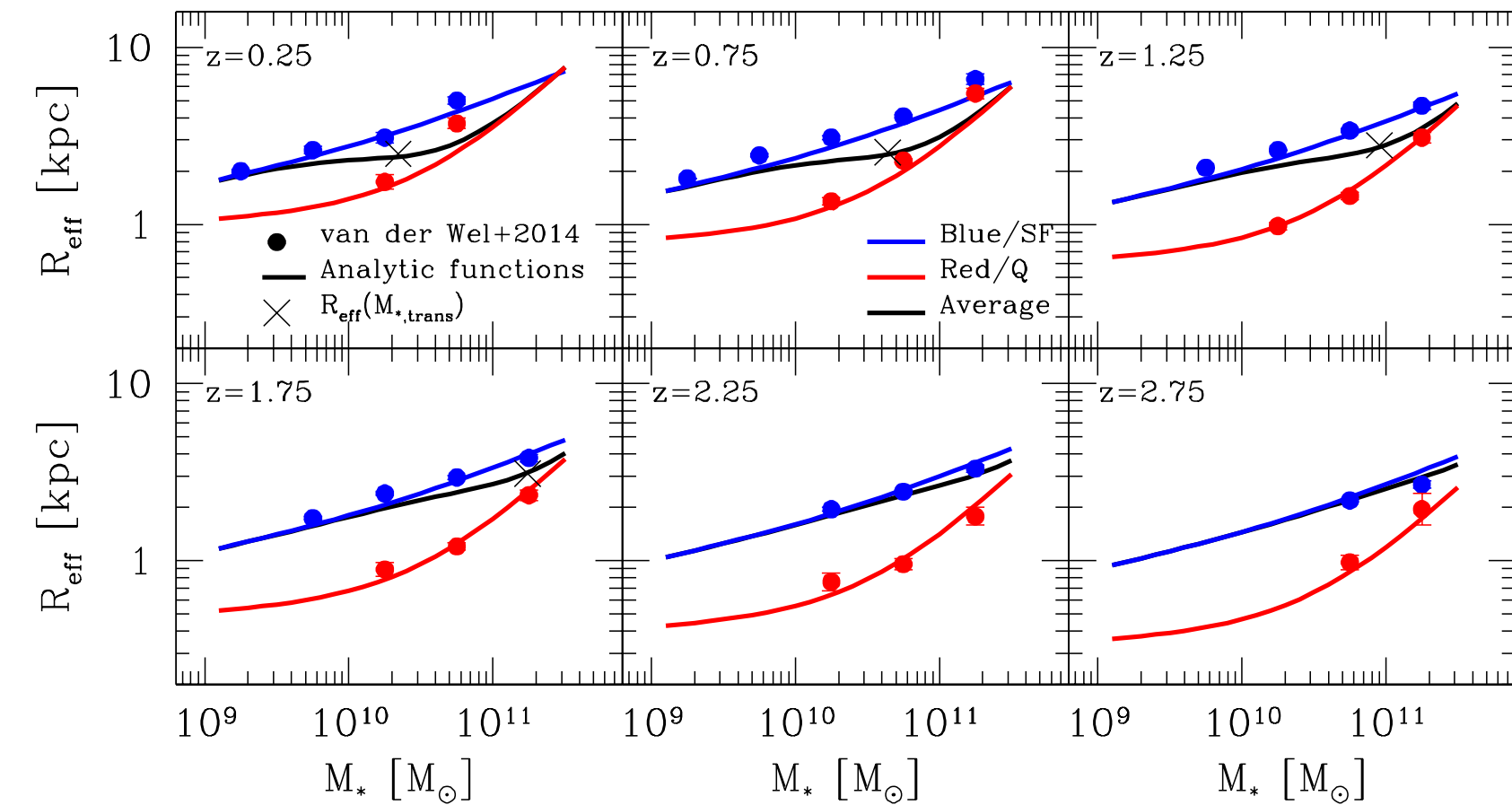


Figure 16. Circularized effective radius for blue star-forming galaxies and red quiescent galaxies for six different redshift bins. The filled circles show the circularized effective radius as a function of stellar mass and redshift from van der Wel et al. (2014) based on multiwavelength photometry from the 3D-HST survey and HST/WFC3 imaging from CANDELS. Solid lines show the redshift dependence for blue and red galaxies of the local relation by Mosleh, Williams & Franx (2013) based on the MPA-JHU SDSS DR7. The black solid lines show the average circularized effective radius as a function of stellar mass. The crosses show the effective radius at  $M_{50}$ , i.e., the stellar mass at which the observed star-forming fraction of galaxies is equal to the quenched fraction of galaxies. Note that the effective radius at  $M_{50}$  evolves very little with redshift and is  $\sim 3$  kpc. We utilize the plotted redshift dependences as an input to derive the average galaxy's radial mass distribution as a function of stellar mass by assuming that blue/star-forming galaxies have a Sersic index  $n = 1$  while red/quenched galaxies have a Sersic index  $n = 4$ .

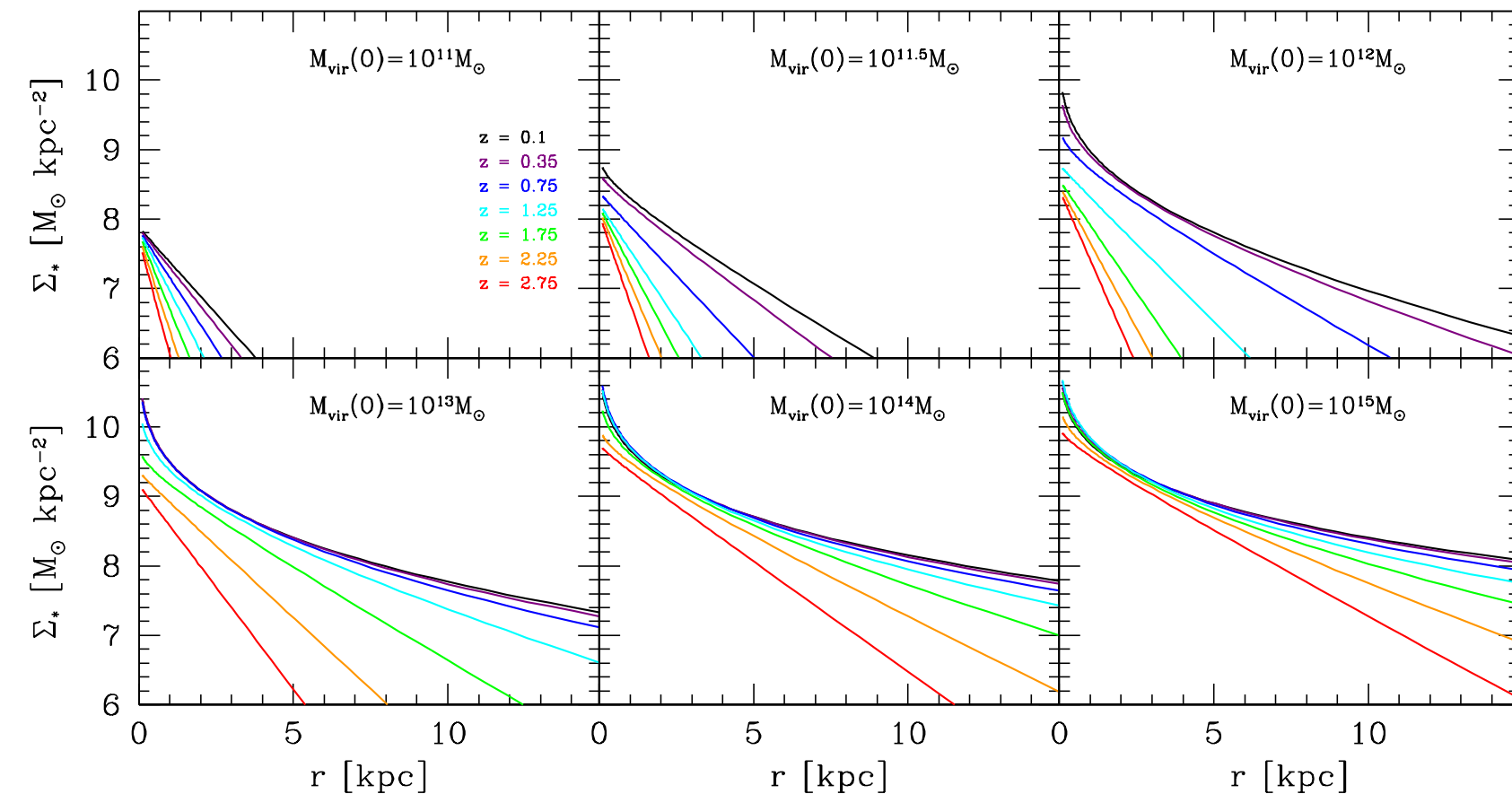
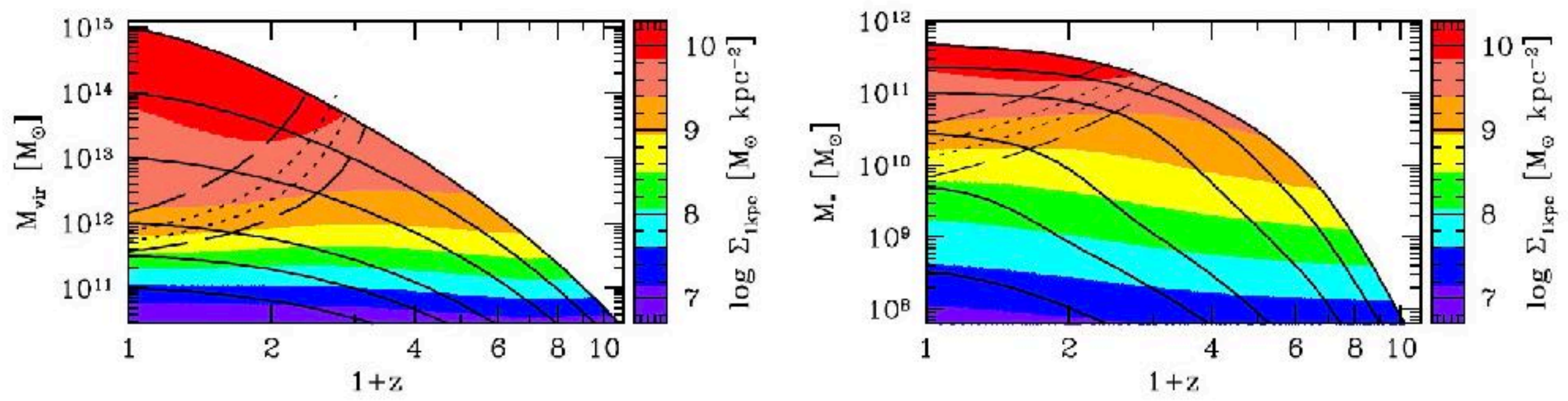


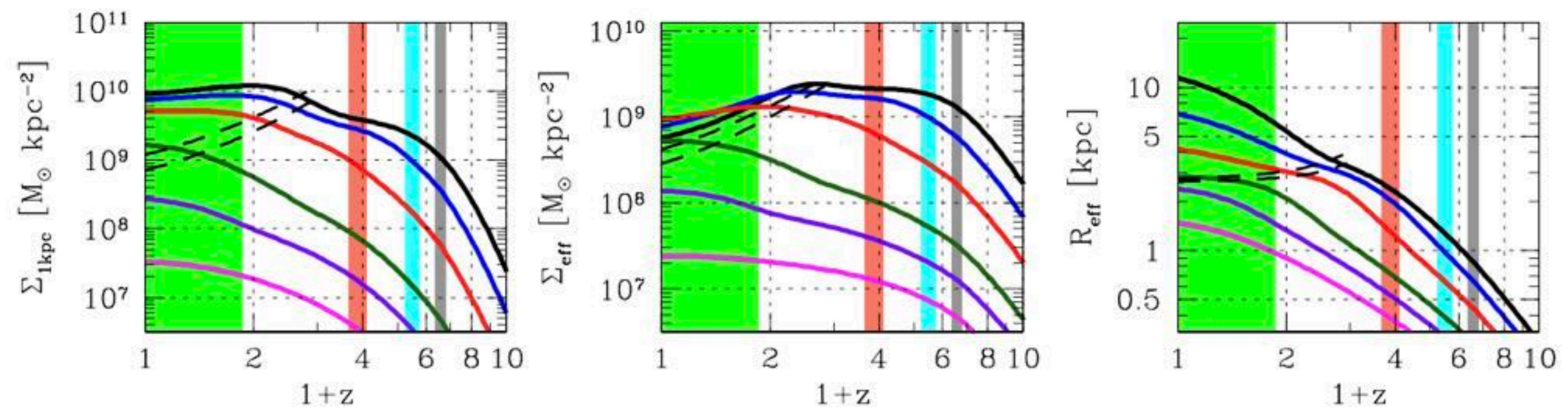
Figure 17. Average evolution of the radial distribution of stellar mass for galaxies in halo progenitors at  $z = 0$  with  $M_{\text{vir}} = 10^{11}, 10^{11.5}, 10^{12}, 10^{13}, 10^{14}$  and  $10^{15} M_{\odot}$ . These radial distributions can be imagined as stacking all the density profiles of galaxies at a given  $z$ , no matter whether galaxies are spheroids or disks or a combination of both.

# Constraining the Galaxy Halo Connection: Star Formation Histories, Galaxy Mergers, and Structural Properties, by Aldo Rodriguez-Puebla, Joel Primack, Vladimir Avila-Reese, and Sandra Faber



This figure (and the left panel below) shows that  $\Sigma_1$  reaching a maximum correlates with quenching:

- $\Sigma_1$  rises steadily toward  $z = 0$  along all progenitor tracks
- $\Sigma_1$  at the quenching transition rises steadily with  $M_{\text{vir}}$  and reaches its maximum at lower redshifts for lower  $M_{\text{vir}}$  — “quenching downsizing”
- The fact that the progenitor tracks are parallel to the trajectory curves shows that  $\Sigma_1$  remains constant after it reaches its maximum



The right panel shows that  $R_{\text{eff}}$  steadily rises along halo trajectories, and quenching typically occurs when  $R_{\text{eff}} \approx 3 \text{ kpc}$ . Although  $\Sigma_1$  is flat after quenching, the middle panel shows that  $\Sigma_{\text{eff}}$  declines after quenching as  $R_{\text{eff}}$  increases.

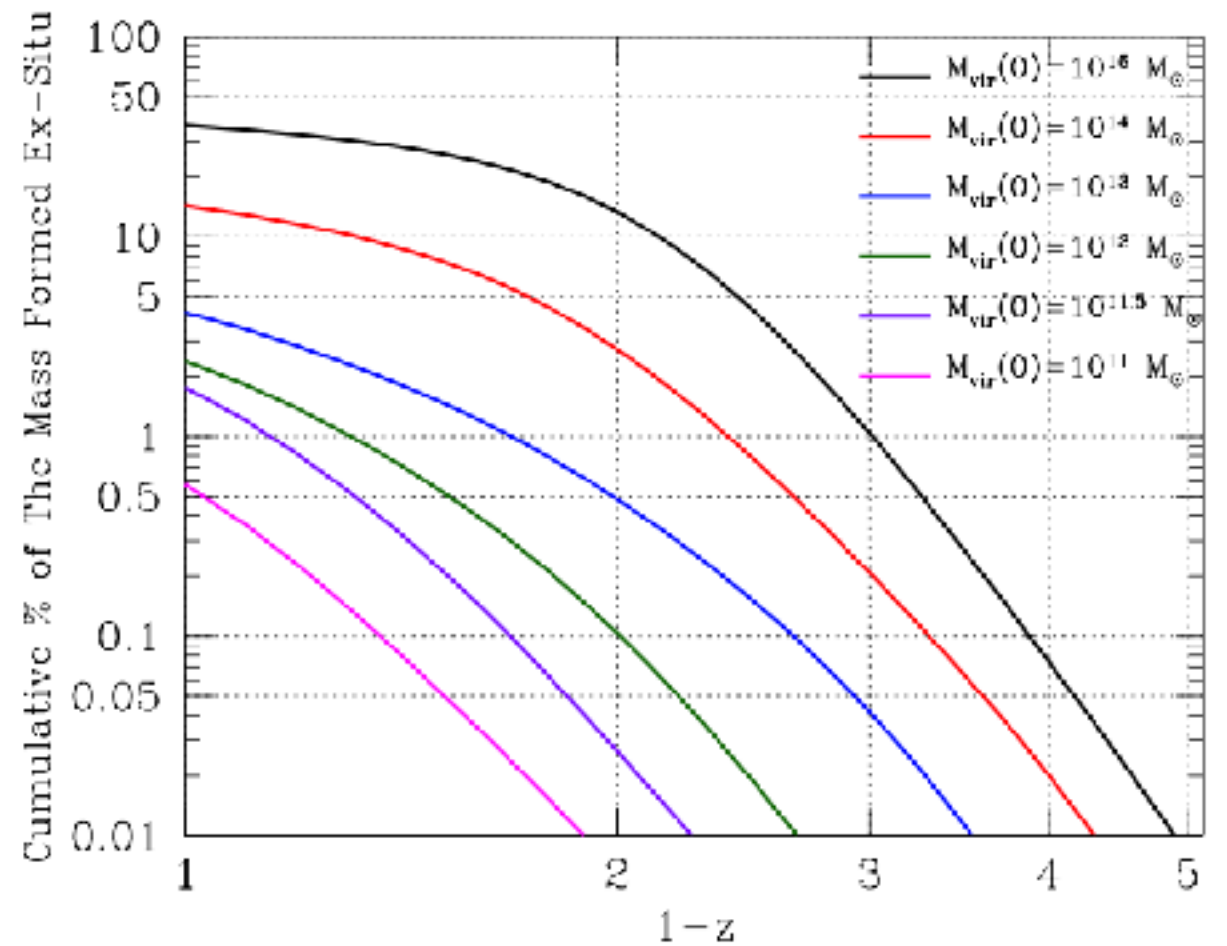
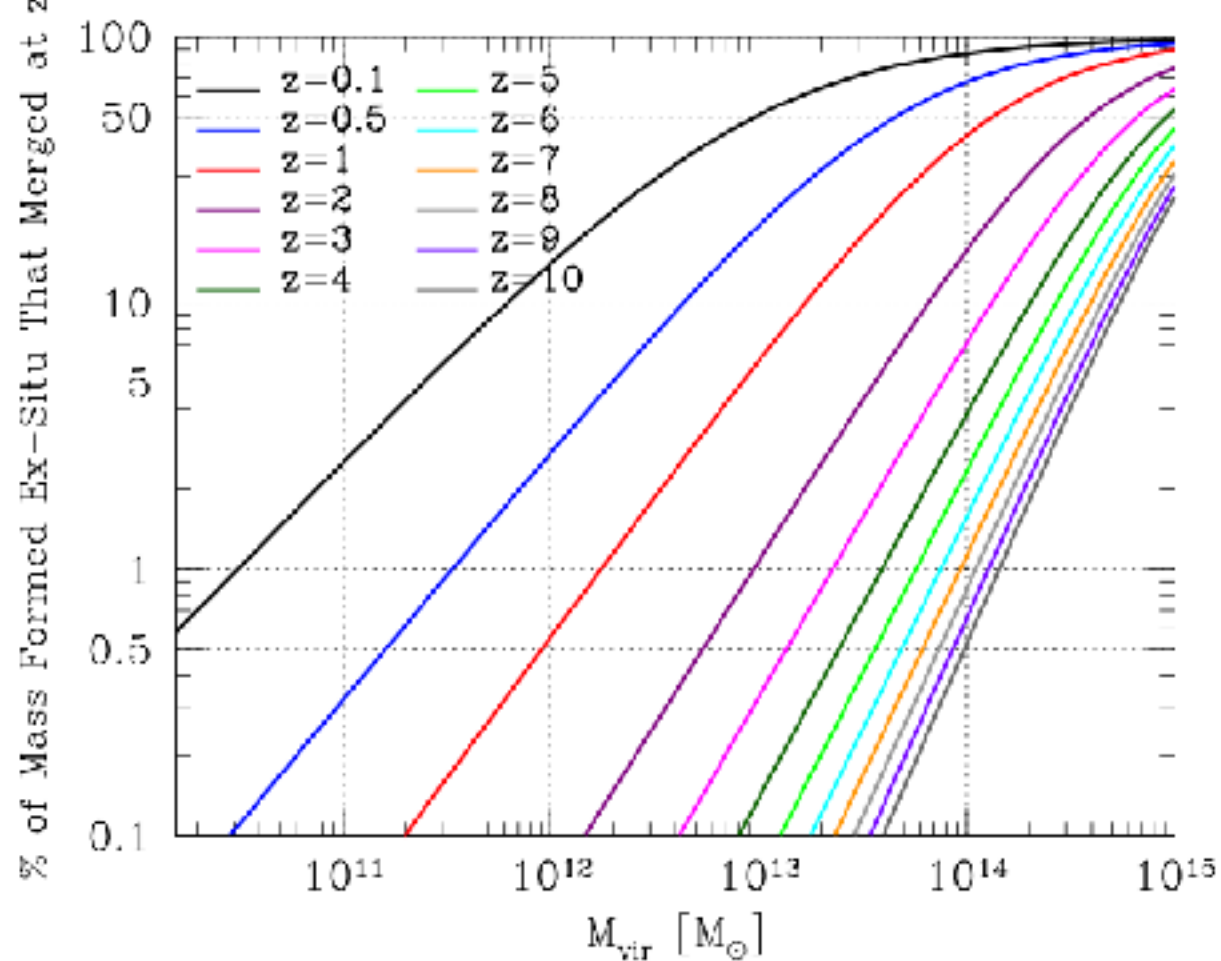


**Figure 13. Left Panel:** Instantaneous fraction of mass that formed ex-situ and was accreted by galaxy mergers as a function of the halo mass at redshift  $z = 0$ . **Right Panel:** Cumulative fraction of mass that formed ex-situ and accreted through galaxy mergers. Note that 40% of the final mass in host galaxies of halos with  $M_{\text{vir}}(0) = 1 \times 10^{15}$  was accreted by galaxy mergers.

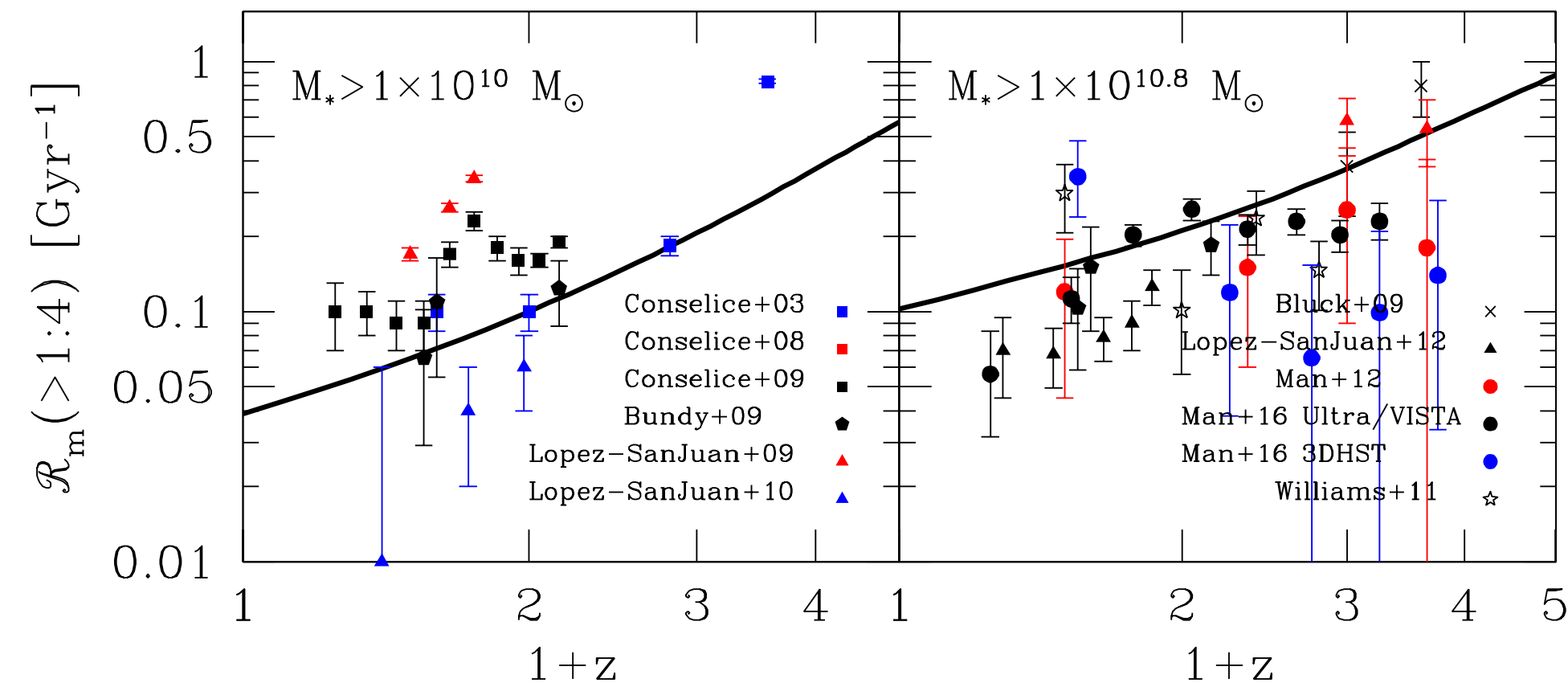


**Figure 14. Left Panel:** Galaxy major merger rate for galaxies with masses above  $1 \times 10^{10} M_{\odot}$ . Solid lines show the predictions based on our new SHMR while the different symbols show observational estimates from Conselice et al. (2003); Conselice, Rajgor & Myers (2008); Conselice, Yang & Bluck (2009); L'opez-Sanjuan et al. (2009) and Lopez-Sanjuan et al. (2010) based on galaxy asymmetries while Bundy et al. (2009) gives the merger rate fraction from galaxy pairs. **Right Panel:** Similarly above but for galaxies with masses above  $1 \times 10^{10.8} M_{\odot}$ . Symbols are from Bluck et al. (2009) using galaxy asymmetries, Lopez-Sanjuan et al. (2012); Man et al. (2012); Man, Zirm & Toft (2016) and Williams, Quadri & Franx (2011) based on galaxy pairs.

There is a tight correlation between the sSFR and  $\Sigma_1$ , in other words,  $\Sigma_1$  is an indicator of the global SFR of the galaxy. Once a galaxy reaches a maximum  $\Sigma_1$ , the SFR is suppressed. The left panel of Figure 19 shows some hints of negative stellar mass evolution within 1 kpc for halos  $M_{\text{vir}} = 10^{14} M_{\odot}$  and  $10^{15} M_{\odot}$ . van Dokkum et al. (2014) reported similar trends based on the analysis of galaxy sizes from the SDSS, Ultra VISTA and 3D-HST surveys.

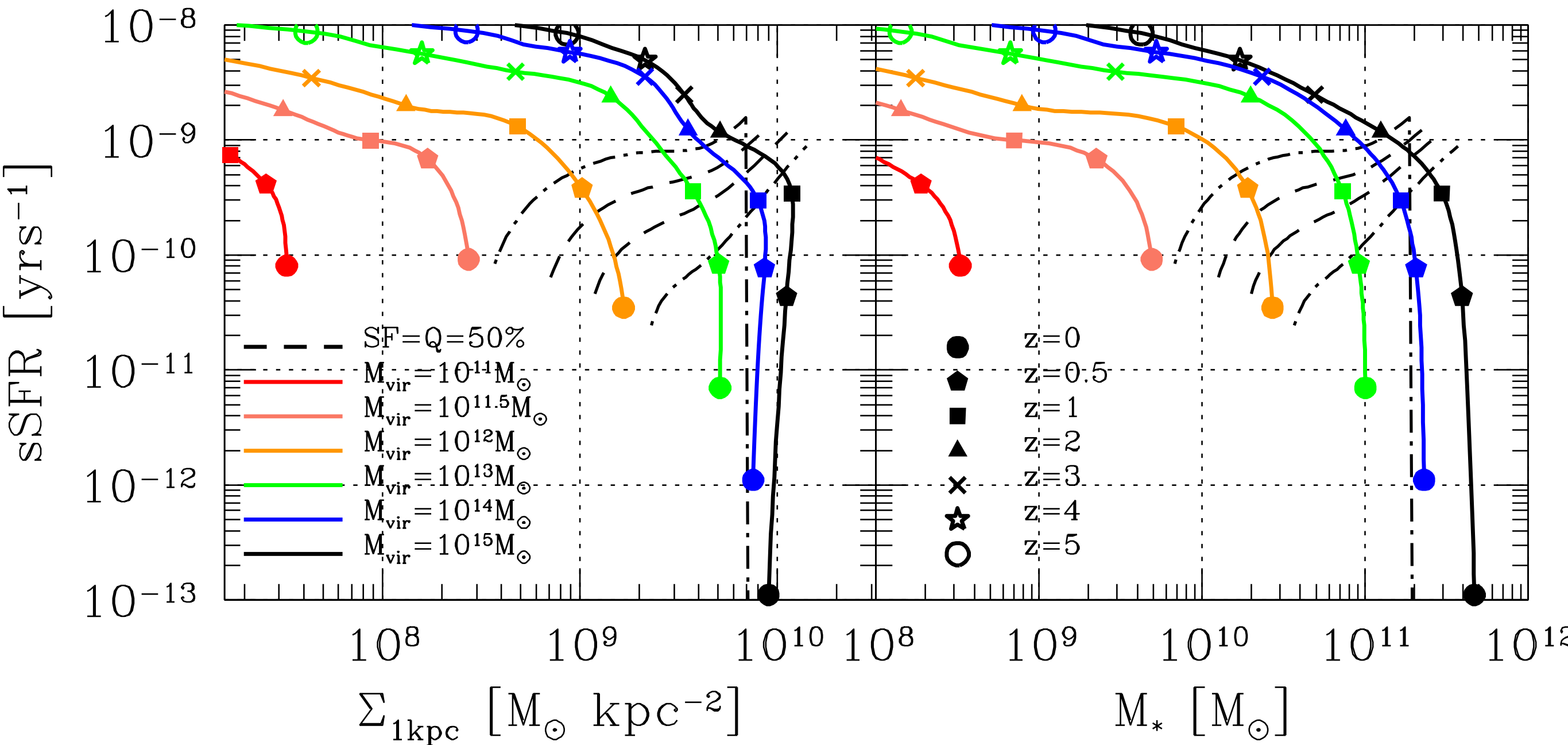
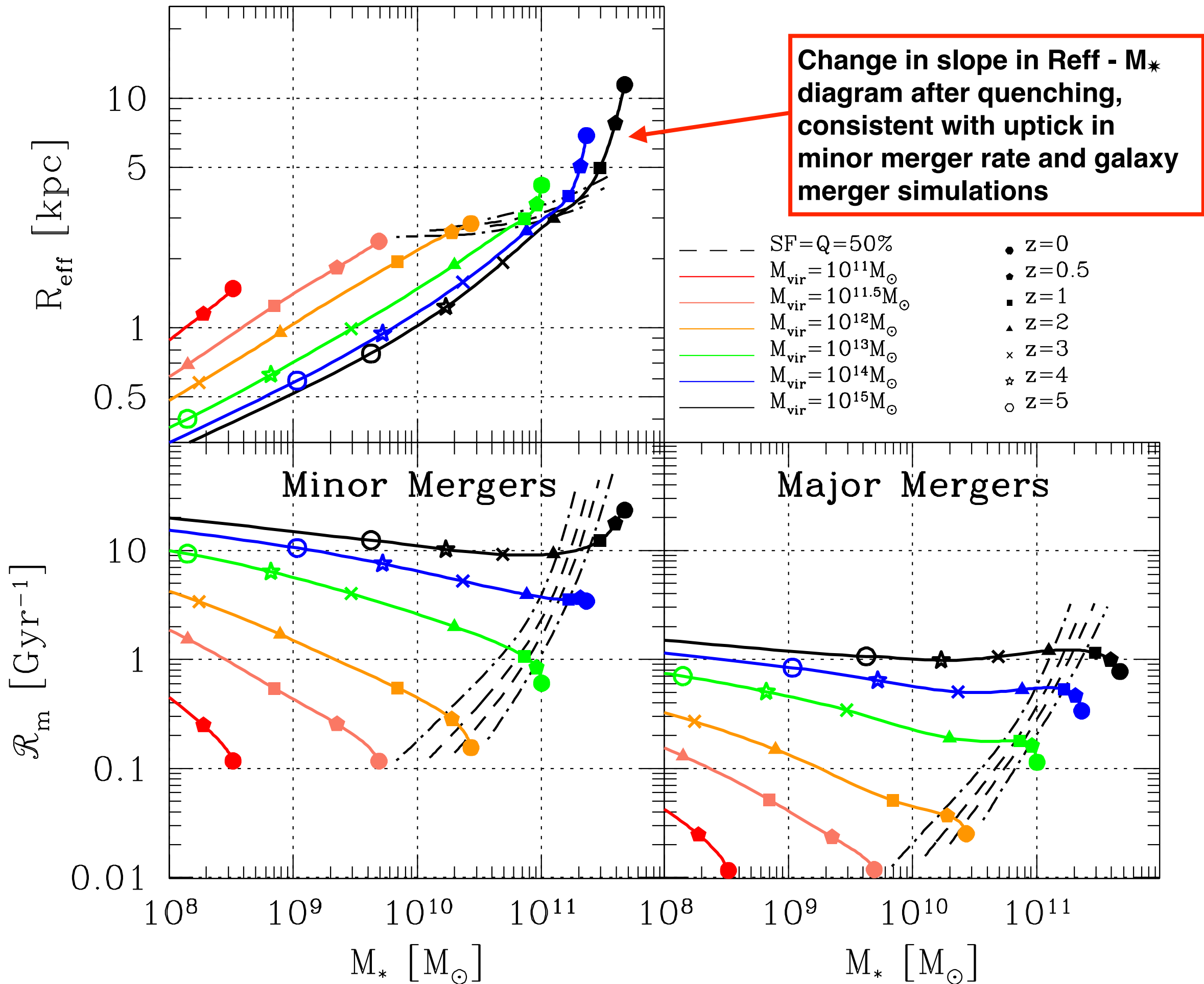


**Figure 19. Left Panel:** Trajectories for progenitors of halos with  $M_{\text{vir}} = 10^{11}, 10^{11.5}, 10^{12}, 10^{13}, 10^{14}$  and  $10^{15} M_{\odot}$  at  $z = 0$  in the  $\Sigma_1$ –sSFR plane. **Right Panel:** Same progenitors but in the  $M_*$ –sSFR plane. The symbols show different redshifts as indicated by the labels. The dashed curves show  $M_{50}(z)$  below which half the galaxies are quiescent, and the upper (lower) dot-dashed curves show where 25% (75%) of the galaxies are quenched.



# Constraining the Galaxy-Halo Connection Over The Last 13.3 Gyrs: Star Formation Histories, Galaxy Mergers and Structural Properties

Aldo Rodríguez-Puebla<sup>1,2\*</sup>, Joel R. Primack<sup>3</sup>, Vladimir Avila-Reese<sup>2</sup>,  
and S. M. Faber<sup>4</sup>

<sup>1</sup> *Department of Astronomy & Astrophysics, University of California at Santa Cruz, Santa Cruz, CA 95064, USA*

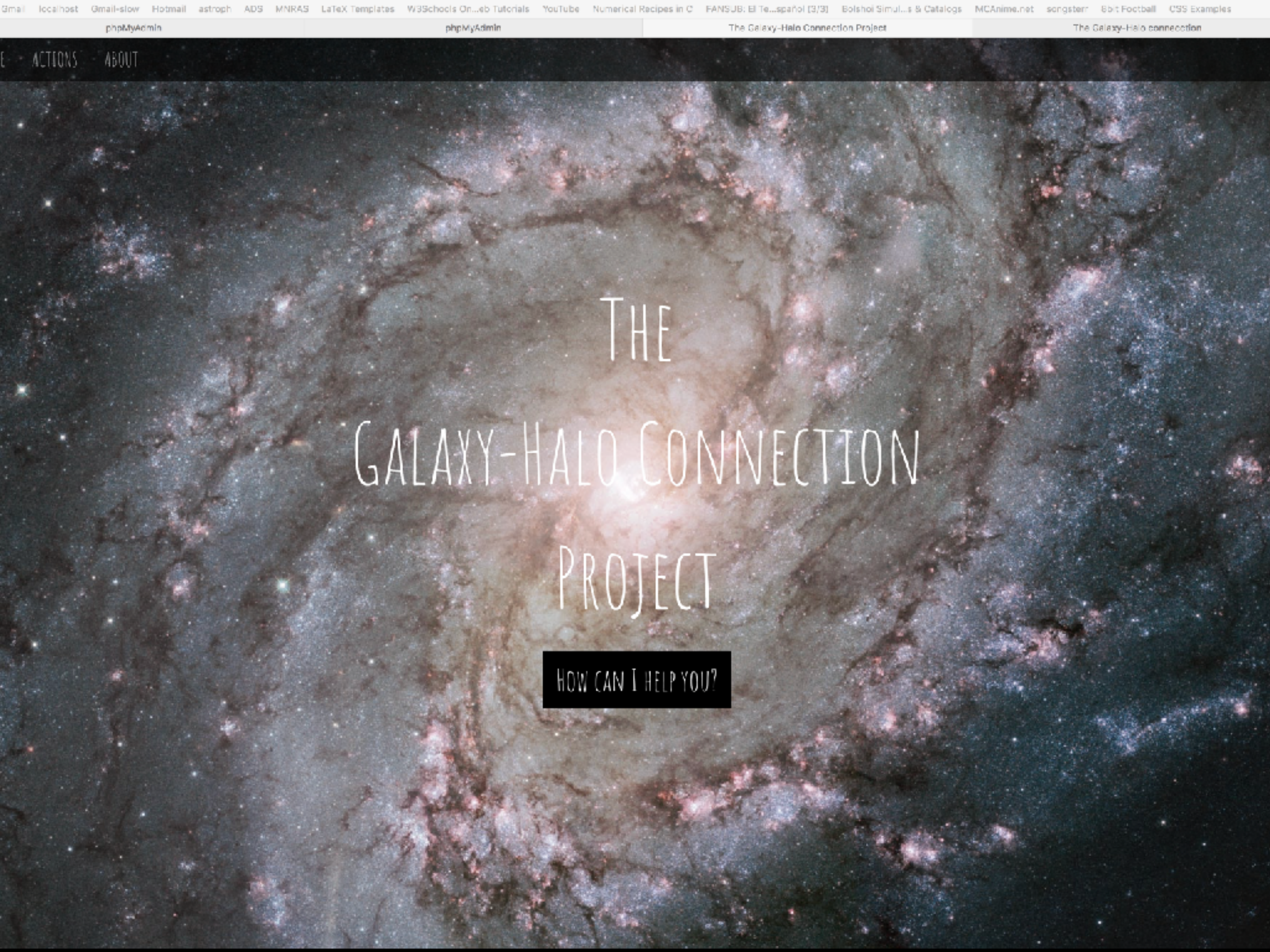
<sup>2</sup> *Instituto de Astronomía, Universidad Nacional Autónoma de México, A. P. 70-264, 04510, México, D.F., México*

<sup>3</sup> *Physics Department, University of California, Santa Cruz, CA 95064, USA*

<sup>4</sup> *UCO/Lick Observatory, Department of Astronomy and Astrophysics, University of California, Santa Cruz, CA 95064, USA*

## ABSTRACT

We present new determinations of the stellar-to-halo mass relation (SHMR) at  $z = 0 - 10$  that match the evolution of the galaxy stellar mass function, the SFR –  $M_*$  relation, and the cosmic star formation rate. We utilize a compilation of 40 observational studies from the literature and correct them for potential biases. Using our robust determinations of halo mass assembly and the SHMR, we infer star formation histories, merger rates, and structural properties for average galaxies, combining star-forming and quenched galaxies. Our main findings: (1) The halo mass  $M_{50}$  above which 50% of galaxies are quenched coincides with  $\text{sSFR}/\text{sMAR} \sim 1$ , where sMAR is the specific halo mass accretion rate. (2)  $M_{50}$  increases with redshift, presumably due to cold streams being more efficient at high redshift while virial shocks and AGN feedback become more relevant at lower redshifts. (3) The ratio  $\text{sSFR}/\text{sMAR}$  has a peak value, which occurs around  $M_{\text{vir}} \sim 2 \times 10^{11} M_{\odot}$ . (4) The stellar mass density within 1 kpc,  $\Sigma_1$ , is a good indicator of the galactic global sSFR. (5) Galaxies are statistically quenched after they reach a maximum in  $\Sigma_1$ , consistent with theoretical expectations of the gas compaction model; this maximum depends on redshift. (6) In-situ star formation is responsible for most galactic stellar mass growth, especially for lower-mass galaxies. (7) Galaxies grow inside out. The marked change in the slope of the size–mass relation when galaxies became quenched, from  $d \log R_{\text{eff}}/d \log M_* \sim 0.35$  to  $\sim 2.5$ , could be the result of dry minor mergers.



# THE GALAXY-HALO CONNECTION PROJECT

HOW CAN I HELP YOU?